REVISTIA

4th International Conference on Medicine and Natural Sciences

Amsterdam, 26-27 April 2019

Venue
Amsterdam Science Park

Conference Proceedings

ISBN 978-164570134-7

REVISTIA

PUBLISHING AND RESEARCH

Amsterdam, 26-27 April 2019

Venue

Amsterdam Science Park

Typeset by Revistia

Printed in Amsterdam

Address: 11, Portland Road, London, SE25 4UF, United Kingdom

Tel: +44 2080680407

E-Mail: office@revistia.com

TABLE OF CONTENTS

The Plasmid Differences in Multi-Drug Resistant Opportunistic Pathogenic Soil Strains of Pseudomonas and Stenotrophomonas

Bella Babayan

Scientific & Production Center "Armbiotechnology", National Academy of Sciences, Republic of Armenia,

National Polytechnic University of Armenia, faculty of Chemical Technologies and Environmental Engineering

Abstract

The antibiotic resistance and especially mult-idrug resistance is one of the most important factors for any microorganism survival in nature. In a majority of cases the resistance to antibiotics, as a property is being defined by several genes which are localized in plasmids, transposons and in other mobile genetical elements. As a result, it has been found out that in some native opportunistic pathogenic soil strains of *Pseudomonas* and *Stenotrophomonas*, the resistance to different antibiotics is caused by simultaneous presence of different plasmids in cells. Besides, the genes of resistance to various classes of antibiotics of I, II, III generations. They can be localized on one plasmid or in more than one plasmids of current bacterial cell. These plasmids of researched strains of *Pseudomonas* and *Stenotrophomonas* are able to stabile replication not only in cells permanently contacting with compatible antibiotic molecules in environment, but also in case of long-term cultivation of bacteria on synthetic media without any antibiotic. The antibiotic resistance of researched *Pseudomonas* and *Stenotrophomonas* strains, which is caused by mobile genetical elements, can be transferred among the microorganisms both in frames of one species and in interspecific and intergeneric gene transfer processes. The plasmids with the presence of genes of resistance to different antibiotics can be transferred to different microorganisms independently, with the forming of new resistant strains, which are differing in resistance to natural antimicrobial organic acidcs as well as their synthetic derivatives and it has a significant ecological and medical importance.

Keywords: Pseudomonas, Plasmids, antibiotics, multi-drug resistance.

Introduction

The antibiotic resistance has an invaluable importance for microbe survival in both nature and clinic under the impact of antibiotics and other effects of anthropogenic influence. The genes of resistance can be localized in both nucleoid (bacterial chromosome) and plasmids or other mobile genetic elements [1]. The presence of them increases adaptivity and the survival probability of microbe in terms of changing conditions of environment. In case of plasmid genes of resistance, this property can be transferred among the microbes by the intraspecific horizontal gene transfer, which can result in formation of new antibiotic resistant strains [2, 3].Different representatives of *Pseudomonas and Stenotrophomonas* are characterized by extremely high level of adaptivity and the presence of various systems of resistance to different classes of antibiotics and other toxic natural and synthetic compounds [4, 5]. They include many multi-drug resistant soil strains which are able to be involved in various ecosystems and forming a quorums, phytopahogenic strains, as well as strains which are opportunistic pathogens of human and animals. They differ by the plasmids and their genes content. The plasmids of *Pseudomonas* can carry the genes of antibiotics modification, efflux system and toxic xenobiotics degradation, up to biodegradation of different cyclic and aliphatic hydrocarbons, toluene derivatives and various wastes of oil production [6-11].

The mentioned above properties can be transferred from one bacteria to other during the process of horizontal gene transfer. And it can become a cause of uncontrolled spread of antibiotic resistance from natural non-pathogenic and conditionally pathogenic bacteria to pathogenic microorganisms in clinics. That is why the research of their genetic mechanisms is very actual in ecological and medial aspects. The main aim of this research was a comparison of genetic mechanisms, which are encoding the properties of multi-drug resistance in different native soil strains of *Pseudomonas and Stenotrophomonas.* Besides, the researched strains and obtained transtformants were compared by their resistance

to newly synthesized derivatives of tartaric acid, which were elaborated and tested in our laboratory, based on literature data about antimicrobial activity of tartaric acid and the derivatives of it [12-14].

Materials and Methods

Cultivation of Cultures

In current research there were used the strains from The National Culture Collection of Microorganisms of the Microbial Depository Center of "Armbiotechnology" Scientific and Production Center National Academy of Sciences, Republic of Armenia: *Pseudomonas aeruginosa, Stenotrophomonas maltophilia (S. maltophilia or former P. maltophilia), P. chlororaphis (subsp. Chlororaphis, subsp. Aurantiaca, subsp. Aureofaciens), P. taetrolens, P. putida, P. fluorescens and P. geniculata*. There were cultivated on liquid and solid agarised media at 37˚C [15].

Atibiotic resistance test

The resistance of all strains was tested by cultivation on agarised cultural media, cotaing 50mkg/ml compatible antibiotic. There were used antibiotics of different classes ad different generations: β-lactamic (Amp/ampicillin, Amx/Amoxicillin, Amc/Augmentin, Cfx/Cefixime and Ctx/Ceftriaxone); aminoglycoside (Kan/kanamycin, Stp/Streptomycin); fluoroquinolone (Cip/Ciprofloxacin); Tcn/Tetracycline, Macrolides (Azm/azithromycin); amphenicol (Cam/Chloramphenicol) produced by "Astoria" [16, 17]. As the control strains there were used *E. coli DH5α* (sensitive to all mentioned above antibiotics)*, E. coli DH5α*/pUC18 (resistant to Ampiciline) and *E. coli DH5α*/VOG 16 (resistant to kanamycin). Antimicrobial activity of Tartaric acid, benzylimide and cyclohexyl amide derivatives was tested according the standard protocols in concentration 1-6% [18].

Analysys of bacterial DNA

The isolation of plasmid and total DNA was carried out by aaalkalie extraxtion method and by the method with the use of benzyl chloride. Then the isolated DNA was researched by 0.8-2.5% agarose gel electrophoresis [19,20]. The transformation of sensitive strains by the plasmid DNA of resistant strains was realized by Mandel's method of competent cells with $CaCl_2$ usage [21-24]. PCR analysis of DNA from the cells of all donor, recipient and transformant strains was done with the following primers: *aph(3')IV, bla$_{OXA}$-10, aac(6')II, pCAT639*: As the marker it was used the standard mix of DNA fragments EcoRI/Hind III [25-28].

Results

The resistance of more than 70 soil strains of 7 species of *Pseudomonas and Stenotrophomonas* to: β-lactamic antibiotics of different generations (Amp, Amx, Amc, Cfx, Ctx); amphenicols (Cam) and aminoglycosides (Stp, Kan) was researched. As a result, the strains which are mono-, multi-drug resistant and sensitive to antibiotics were detected. One part of them was resisrant not only to β-lactamic antibiotics, but also the growth of them couldn't be inhibited by to clavulanic acid of augmentin. Then the DNA samples were isolated from all strains and the plasmid content of their cells was compared.

The identification of resistance genes was done by PCR analysis. For the definition of resistance genes localization, the sensitive strains *P. aeruginosa 9056* and *E. coli DH5α* were transformed by the plasmids from the resistant strains and then the transformed strains were selected on different selective media with compatible antibiotics (Table 1).

During the experiments it was found out that for 4 strains, the resistance of transformants differed from the donor's resistance. The resistance of *P. aeruginosa 9056* and *E. coli DH5α* transformed by the same plasmids was identical. The correlation between transformation and PCR analysis data are presented in Table 2.

The results of antimicrobial effect differences while tests with derivatives of tartaric acid are shown on Table 3.

Discussion

As it was shown above, in resistant stain *P. aeruginosa 9059* two different plasmids were detected. In one of them acetyl-Co-A-dependent aminoglycoside N-acetyltransferase gene *aac (6') II,* which defined the resistance to Kan, was identified.

The gene of chloramphenicol acetyltransferase CatB7 *pCAT639* is identified in bacterial chromosome and that is why this property cannot be transferred, just as the resistance to Stp, which is encoded by chromosomal genes too. The second plasmid of this strain contains the genes of resistance to β-lactamic antibiotics. Both plasmids can transfer the resistance to other microorganisms by intraspecific horizontal gene transfer [29]. According to the collected data, the cells which were transformed by the plasmids of multi-drug resistant strain *P. aeruginosa 5249,* containing blaOXA10 β-lactamase gene

bla$_{OXA}$10, *pCAT639* and ATP-dependent aminoglycoside O-phosphotransferase gene *aph (3') VI,* were sensitive to Stp and Cam. It is caused by the plasmid localization of genes *bla$_{OXA}$10* and *aph (3') VI* and chromosomal localization of *pCAT639* [30, 31].

In *S. maltophilia 306d2* – there were detected 2 types of plasmids, which can be transferred separately. In one of them the gene *blaOXA10,* while in the second one gene *aph (3') VI* are identified. Probably, the resistance to both aminoglycosides and β-lactams, which was detected for one type of transformants, containing this plasmid, is caused by the genes of another lactamase or efflux system [32]. In *S. maltophilia 9289* the genes *bla$_{OXA}$10* and *aac (6') II* were detected on different plasmids which could be transferred independently, while the resistance to Cam was defined by chromosomal genes. Accordig to data from table 3, the transformants, which were selected on aminoglycosides are more resistant. Thus probably, thy plasmids of these strains carry additional genes of degradation or efflux of tartaric acid and the derivatives of it, whike the plasmids with genes of resistance to β-lactamic antibiotics have no relation to this property.

Conclusion

As the result of experiments among the researched multi-drug resistant microbes, the strains with different plasmids and more than one plasmid simultaneously were detected. These plasmids carry different genes of resistance to β-lactams and aminoglycosides and are able to stable replication even after the long-term cultivation on media without antibiotics. The resistance to chloramphenicol in all these strains is caused by chromosomal genes. In some cases, the resistance to β-lactams is caused by both chromosomal and plasmid genes. For 2 strains of *P. aeruginosa* and 2 strains of *S. maltophilia* an ability to transfer the resistance to aminoglycosides and to β-lactams independently by 2 different plasmids with additional genes of resistance to natural aldaric acids like tartaric acid, by the intraspecific horizontal gene transfer, was shown and it has a huge ecological significance for new antibiotic resistant strains formation and spread in nature.

This work was supported by the RA MES State Committee of Science, in the frames of the research project № 18T-2I036.

References

[1] Li E. Zh., Dawei Zh. D. X., Jin X., Chunguang Y., Hao F., Zhouhua J., Li X., Tingyue G., Ke Y. (2016, February) Microbiologically Influenced Corrosion of 2707 Hyper-Duplex Stainless Steel by Marine *Pseudomonas aeruginosa* Biofilm Huabing, Sci Rep., 6 (20190).

[2] Felker P, Medina D, Soulier C, Velicce G, Velarde M, Gonzalez C. (2005, April) A survey of environmental and biological factors (*Azospirillum spp., Agrobacterium rhizogenes*, *P. aurantiaca*) for their influence in rooting cuttings of Prosopis alba clones. J Arid Environ. 61 (2): 227–247.

[3] Dashchyan N.A., Asatryan N.L., Galstyan G.F., Mikaelyan A.R. (2014, November), Obtaining Bioactive Additives of Cyclic Structure on the Basis of Optically Active Tartaric Acid. Bulletin of NPUA, Collection of scientific papers, part II, pp. 682-68CLSI,

[4] Gharajyan S.K, Babayan B.G., Sogomonyan T.M., Mikaelyan A. R, Melkumyan M.A., Baghdasaryan A. S. (2018, November), The Influence of Tartaric Acid and The Derivatives of It On Some Soil Non Pathogenic Strains of Pseudomonas, The materials of Conference: "The Assessment of Biodiversity and Agro-Biodiversity Capacity of the RAand the Implementation of the Scientific-Educational Foundation for Biodiversity Conservation", ASPU, 1(1), 171-174

[5] Performance Standards for Antimicrobial Susceptibility Testing (2017, January), Suplement M100S, 27th ed.

[6] CMI, ESCMID, ECAST, Terminology relating to methods for the determination of susceptibilityof bacteria to antimicrobial agents (2010, May), ESCMID 6, 4503-508.

[7] Lucotte G., Baneyx F. (1993). Introduction to Molecular Cloning Techniques. Wiley-Blackwell. p. 32. ISBN 978-0471188490.

[8] Blanco P., Hernando-Amado S., Reales-Calderon J.A., Do Corona F., Lira F., Alcalde-Rico M., Bernardini A., Sanchez M. B., Martinez J. L. (2016 March) Bacterial Multi-drug Efflux Pumps: Much More Than Antibiotic Resistance Determinants, Microorganisms. 4(1): 14.

[9] Maurya A. P., Dhar D., Basumatary M. K., Paul D., Ingti B., Choudhury D., Talukdar A. D., Chakravarty A., Mishra S., Bhattacharjee A. (2017,April) Expansion of highly stable blaOXA-10 β-lactamase family within diverse host range among nosocomial isolates of Gram-negative bacilli within a tertiary referral hospital of Northeast India", BMC Res Notes. 10(1):145..

[10] Xiumei H., Banglao X., Yinmei Y., Liu D., Yang M, Wang J., Shen H., Zhou X., Ma X. (2013, March) A high throughput multiplex PCR assay for simultaneous detection of seven aminoglycosideresistance genes in *Enterobacteriaceae*, Hu et al. BMC Microbiology, 13, 58.

[11] Jovcić B, Lepsanović Z, Begović J, Rakonjac B, Perovanović J, Topisirović L, Kojić M. (2013, July)The clinical isolate *Pseudomonas aeruginosa* MMA83 carries two copies of the blaNDM-1 gene in a novel genetic context." Antimicrob Agents Chemother, 57(7):3405-7.
[12] Tanner W.D, Atkinson RM, Goel R.K., Toleman M.A, Benson LS, Porucznik CA, VanDerslice JA. (2017, April) Horizontal transfer of the *blaNDM-1* gene to *Pseudomonas aeruginosa* and *Acinetobacter baumannii* in biofilms." FEMS Microbiol Lett, 364(8).
[13] Rampioni G., Pillai C. R., Longo F., Bondì R., Baldelli V., Messina M., Imperi F., Visca P., Leoni L. (2017, September) Effect of efflux pump inhibition on *Pseudomonas aeruginosa* transcriptome and virulence, Sci Rep., 7: 11392
[14] Heng Zhu, Feng Qu, Li-Huang Zhu. (1993, November) Isolation of Genomic DNA From Plants, Fungi and Bacteria Using Benzyl Chloride. Nucleic Acid Research, 21 (22), 5279-5280.
[15] Viovy J.-L. (2000, July). Electrophoresis of DNA and other polyelectrolytes: Physical mechanisms. Reviews of Modern Physics. 72: 813–872.
[16] S. Eswaranandam N. S. Hettiarachchy M. G. Johnson (2004, April), Antimicrobial Activity of Citric, Lactic, Malic, or Tartaric Acids and Nisin-incorporated Soy Protein Film Against Listeria monocytogenes, Escherichia coli O157:H7, and Salmonella gaminara, Journal of Food Science, 69(3), FMS79-FMS84
[17] Wang J, Liu J.-H. (2004 June) Mutations in the chloramphenicol acetyltransferase (S61G, Y105C) increase accumulated amounts and resistance in *Pseudomonas aeruginosa*, School of Life Science & Technology, Shanghai Jiaotong University, No. 800, China Received, 197-204.
[18] Madigan M, Martinko J. (2005, January) Brock Biology of Microorganisms. (11th ed.). Prentice Hall. ISBN 0-13-144329-1.
[19] Haas D, Défago G. (2005, May) Biological control of soil-borne pathogens by fluorescent pseudomonads. Nat Rev Microbiol. 3(4):307-19.
[20] Shen JP, Zhang LM, Zhu YG, Zhang JB, He JZ. (2008, June) Abundance and composition of ammonia-oxidizing bacteria and ammonia-oxidizing archaea communities of an alkaline sandy loam., Environ Microbiol., 10(6):1601-11.
[21] Kaiser S., Biehler K., Jonas D. (2009, May) A Stenotrophomonas maltophilia Multilocus Sequence Typing Scheme for Inferring Population Structure, J Bacteriol., 191(9): 2934–2943.
[22] Singh M., Yadav A., Ma X., Amoah E. (2010, April) Plasmid DNA Transformation in *Escherichia Coli*: Effect of Heat Shock Temperature, Duration and Cold Incubation of CaCl 2 Treated Cells, International Journal of Biotechnology and Biochemistry, 6 (4), 561–568
[23] Marcelletti S, Scortichini M. (2014, December) Definition of Plant-Pathogenic *Pseudomonas genomospecies* of the *Pseudomonas syringae* Complex Through Multiple Comparative Approaches, Phytopathology, 104(12): 1274-82.
[24] Lee J., Zhang L. (2015, January), The hierarchy quorum sensing network in *Pseudomonas aeruginosa*, Protein Cell, 6(1): 26–41.
[25] S.S. Hoseini and M. G. Saue (2015, January) Molecular cloning using polymerase chain reaction, an educational guide for cellular engineering, J. Biol Eng., 9, 2.
[26] Silva M.M., Lidon F.C (2016, January), An overview on applications and side effects of antioxidant food additives, Emirates Journal of Food and Agriculture, 28(12): 823-832
[27] Lateef B. Salam (2016, June) Metabolism of waste engine oil by *Pseudomonas* species. 6 (1) doi: 10.1007/s13205-016-0419-5.
[28] Liu Y, Wang H, Cui T, Zhou X, Jia Y, Zhang H, He ZG (2016, July) NapM, a new nucleoid-associated protein, broadly regulates gene expression and affects mycobacterial resistance to anti-tuberculosis drugs.", Mol Microbiol.,101(1):167-81.
[29] Rohde A., Hammerl J.A., and Dahouk S. A. (2016, September). Rapid screening for antibiotic resistance elements on the RNA transcript, protein and enzymatic activity level, Ann Clin Microbiol Antimicrob, 5 (55), 2-8, DOI 10.1186/s12941-016-0167-8.
[30] Baumrin E, Piette E.W., Micheletti R.G (2017, December) *Stenotrophomonas maltophilia*: an emerging multi-drug resistant opportunistic pathogen in the immunocompromised host., BMJ Case Rep. pii: bcr-2017-221053.
[31] Subedi D, Vijay A.K., Willcox M. (2018, March) Overview of mechanisms of antibiotic resistance in *Pseudomonas aeruginosa*: an ocular perspective, Clin Exp Optom.; 101(2):162-171,
[32] S. Delaney, R. Murphy, F. Walsh (2018, August) A Comparison of Methods for the Extraction of Plasmids Capable of Conferring Antibiotic Resistance in a Human Pathogen From Complex Broiler Cecal Samples, Front Microbiol. 9: 1731

[33]

Table 1. Sensitive strains transformation by plasmid DNA of resistant strains.

(R- resistance; S- sensitivity; + the growth on media; - the absence of growth).

Donor and the antibiotic of election	Donor's Resis-tance	Resistance of transformants							
		Amp	Amx	Amc	Cfx	Ctx	Kan	Stp	Cam
P. aeruginosa 5249 (on β-lactams, Cam & on aminoglycosides)	R, Azm^S	+	+	+	+	+	+	-	-
P. aeruginosa 9059 (on β-lactams, Cam)	R, Stp^S, Ctx^S	+	+	+	+	-	-	-	-
P. aeruginosa 9059(on Kan)		-	-	-	-	-	+	-	-
S. maltophilia 306d2(on β-lactams, Cam)	R, Cam^S	+	+	+	-	-	-	-	-
S. maltophilia 306d2 (on aminoglycosides)		+	+	+	-	-	+	-	-
S. maltophilia 9289 (on β-lactams, Cam)	R	+	+	+	-	-	-	-	-
S. maltophilia 9289 (on aminoglycosides)		-	-	-	-	-	+	-	-

Table 2. Correlation between PCR analysis and plasmid consistence of cells.

(R- resistance; S- sensitivity; + the growth on media; - the absence of growth).

Pseudomonas	Resistance	Plasmids	PCR
P. aeruginosa 9059	R, Ctx^S	2 plasmids	aac (6') II – 2,2kb pCAT639 - 1,4kb
P. aeruginosa 5249	R, Azm^S	1 plasmid	bla_{OXA}10-1,6kDa aph (3') VI– 2kDa pCAT639-*1,4kDa*
S. maltophilia 306d2	R, Cam^S	2 plasmids	*bla_{OXA}10* - 1,6kb aph(3')VI– 2kDa
S. maltophilia 9289	R	2 plasmids	*bla_{OXA}10* - 1,6kb *aac (6') II* - 2,2kb

Table 3. Antimicrobial effect of tartaric acid and the derivatives of it on obtained transformant strains of Pseudomonas and Stenotrophomonas, which were selected on different antibiotics.

(Na_2-TA – Disodium salt of L- tartaric acid, Na/K-TA – Sodium potassium L(+)-tartrate tetrahydrate, TA – L-Tartaric Acid, CHA – NH_4^+-salt of Cyclohexyl amide of L-tartaric Acid, BATA – NH_4^+-salt of Benzilimide of L-Tartaric Acid, C – Control sample on Agarised cultural media, + the growth of bacteria on media; - the absence of growth of bacteria on media).

Strain of bacteria	Testing Antimicrobial compound					
	Na_2-TA	Na/K-TA	TA	BATA	CHATA	C
P. aeruginosa 5249 (on β-lactams, Cam & on aminoglycosides)	+	+	+	-	-	+
P. aeruginosa 9059 (on β-lactams, Cam)	+	+	+	-	+	+
P. aeruginosa 9059 (on Kan)	-	+	-	+	-	+
S. maltophilia 306d2 (on β-lactams, Cam)	-	-	+	-	-	+
S. maltophilia 306d2 (on aminoglycosides)	-	-	+	-	-	+
S. maltophilia 9289 (on β-lactams, Cam)	+	+	+	-	-	+
S. maltophilia 9289 (on aminoglycosides)	+	+	+	+	+	+

The Research of Dynamics of Immune Responsibility Indicators in Patients with Epstein–Barr Virus (EBV) Infections

T. I. Liadova

K. V. Pavlikova

V. N. Karazin Kharkiv National University, Kharkiv, Ukraine

Abstract

The main task of modern infectious immunology is the elucidation of immunopathogenetic mechanisms of the unfavourable course of the disease. The course of the infectious process caused by the viruses and the microorganisms factors. At the heart of the complicated flow or chronicity of the process is an ineffective immune response that is not able to prevent the dissemination of the virus or the complete elimination of the pathogen from the body, which is the cause of the formation of relapses or chronic course of the disease. In the modern literature, there is evidence that in patients who have suffered from infectious mononucleosis (IM), regardless of the severity of the disease, a secondary immunodeficiency develops, which is the cause of possible bacterial complications. After IM is not always observed update of the immune balance and changes in the hemogram staying for a long time.

Keywords: research, dynamics, immune, responsibility, indicators, patients, epstein–barr virus, EBV, infections

Introduction

Immunological status of patients with IM has a number of features. The essence of the general pattern of changes is to increase the number of T- and B-lymphocytes at the MI, and in the subpopulation of T-lymphocytes, an increase in the number of cytotoxic cells, which makes it possible to regard the IM as a lymphoproliferative process. Increasing the level of T lymphocytes with suppressor activity is one of the main regulatory mechanisms for suppressing the early stages of B-lymphocyte expression, both directly acting on them and indirectly, inhibiting the activation of T-helper cells. In turn, the reduction of T-helper cells leads to blockage induction of apoptosis. Consequently, with IM there is a slowdown in apoptosis of "exhausted" effector cells and there is no impediment to their participation in the immune response. Ultimately, with EBV infection, the probability of occurrence of auto-reactive, as well as malignant cell clones may appear. A number of researchers note from the side of the humoral link immunity increase the amount of IgA and IgM, which is characteristic of severe forms of MI.

In addition, many researchers are actively studying the relationship between the severity of the course and individual indicators of the immune system. At the primary infection, neutralizing antibodies, antibodies of IgM and IgG antibodies to VCA are formed, and later to EA and NA antigens of EBV. It is believed that the mild IM is associated with an effective immunological defence of the T cell line of immunity and a high level of α-IFN. The severe course of the infection is due to insufficiency of both the cellular and humoral immunity, accompanied by low concentrations of α-IFN, the reversal of IFN products from α to γ-type and violation of the elimination of common CIC.

The number of studies devoted to the study of the nature of immune disorders of laboratory manifestations of IM depending on the stage of the infectious process in adult patients in our country is very limited. It also needs to clarify the diagnostic significance of specific methods of ELISA and PCR in different stages of the infectious process.

The aim of the study. To investigate the nature and extent of immune status disorders in patients with acute EBV infection.

Materials and methods. To accomplish our research objectives, we examined 60 patients with IM.

The diagnosis of IM in patients under our supervision was based on clinical, anamnestic and laboratory data. All patients have undergone a medium-severe form of IM.

The complex of patients' examination included clinical analysis of blood, detection of atypical mononuclear cells, determination of specific Ig to the EBV by solid-phase immunoassay, detection of the DNA of the EBV by polymerase chain reaction (PCR) in blood and saliva in the dynamics of the disease. In order to confirm the diagnosis, in addition to the general analysis of blood, a series of serological and molecular genetic studies were performed. As a screening rapid blood test for the presence of EBV infection, a heterophilic test in the Hoff-Bauer modification was used (Chirekskina, 1973).

The blood lymphocyte phenotype was determined using a flow-through laser cytometry on a FACS-Calibur (USA) apparatus using monoclonal antibodies (Dumbaeva, 2002; Hanunova, 1999). For identification on the cells of CD3 +, CD4 +, CD8 +, CD16 +, CD20 +, CD25 +, CD8 + CD28 +, CD8 + CD28-, appropriate antibodies labelled with FITC were used. The monoclonal antibodies INFγ-RS-5, IL-4-PE, TFRβ-FITC (eVioscience, Beckman) were used to identify the TF lymphocytes INFγ (Th1-cells), IL-4 (Th2-cells) TFRβ1 (Th3-cells) (eBioscience, Beckman Caulter, R&D System). All stages of preparation of samples for laser cytofluorometry were conducted in accordance with the protocols of the manufacturer. The method of simple radial immunodiffusion in a gel was used to study the content of Ig classes A, M, G in serum.

The results of the research were processed by the method of variation and correlation statistics using the program "Statistic 10.0 for Windows". For each variation series, the average arithmetic (M), mean square deviation (σ), average error of the arithmetic mean (m) was calculated. Methods of parametric and nonparametric statistics were also used. Quantitative and qualitative analysis of intra-system and inter-system correlation connections was carried out using the method of correlation structures and the sequential analysis of Wald.

Results of the research. The complex analysis of the state of the immune response, its nature and intensity, the balance of the subpopulations of the reactive cells, and the production of immunoregulatory molecules is of great importance in the study of pathogenesis and clinics of the EBV infection, which ultimately helps identify the antiviral strategy of the organism.

The subpopulative composition of the main lymphocytes, as well as the indicators reflecting the state of the humoral immune response - the content of CIC and IgA, M, G was studied in the peripheral blood of patients with IM in the dynamics of the disease - in the period of rapid and convalescence (before discharge from the hospital). The results are shown in table 1.

The analysis of the results of the study on the content of relative and absolute indices of the major subpopulations of lymphocytes revealed the heterogeneity of the content of these immunocompetent cells in the period of the onset of the disease. As can be seen from table 1, the subpopulation composition of lymphocytes in the group of patients with IM was characterized by certain qualitative and quantitative differences compared with the control group.

Thus, during the acute period of IM in the peripheral blood of patients due to high content of leucocytes observed significant increase of the relative and absolute number of some subpopulations of lymphocytes compared with the data of the control group patients.

Thus, in patients with IM, the increase in content [$CD3^+$ – 87.21±3.34%; $CD4^+$ – 47.16±1.07%; $CD8^+$ – 44.16±3.78%; $CD16^+$ – 16.61±0.6; $CD20^+$ – 18.91±0.9%; $CD8^+CD28^+$ – 17.6±1.1%; $CD25^+$ – 21.4±1.92%], ($p<0.05$) compared with similar parameters of the control group [$CD3^+$ – 65.85±3.5%; $CD4^+$ – 42.0±1.31%; $CD8^+$ – 29.4±1.9%; $CD16^+$ – 14.52±0.44%; $CD20^+$ – 13.5±0.5%; $CD8^+CD28^+$ – 14.8±0.9%; $CD25^+$ – 16.0±1.45%] ($p<0.05$) was exceeded. The increase in Th1-cell content was also observed in probability and was 15.2±0.94% versus 11.1±1.1% ($p<0.05$). The values below the control values were $CD8^+CD28^-$, which did not differ from the control values – 5.7±0.3% ($p>0.05$), and the Th2-cell content tended to decrease: 10.4±1,78 versus 12.4±1.43 ($p>0.05$), respectively.

Thus, the study of the phenotypic spectrum of lymphocytes showed an increase in the content of mature T-lymphocytes ($CD3^+$), cytotoxic T-suppressor cells ($CD8^+$), cells expressing the activation marker $CD25^+$ (receptor IL-2). The imbalance in the ratio Th1/Th2 ($p<0.001$), due to an increase in the relative content of Th1-cell Th-lymphocytes, confirms that the effective protection and elimination of the pathogen is formed by transforming the T-helper response toward Th1 cells. In addition, an increase in the number of lymphocytes that carry the receptor to IL-2 ($CD25^+$) in the acute period is evidently indicative of activation of the immune system and an increase in the number of cells that respond to IL-2.

In the period of convalescence, a probable reduction was observed only with respect to the relative content of lymphocytes from 57.67±2.81 to 45.65±2.32% and 5.74±0.65 to 3.6±0.38 x 10^9 ($p<0,05$), the index of $CD3^+$ was 87.21±3.34 to 79.21±2.29% ($p<0.05$).

Table 1. **Subpopulation of lymphocytes of peripheral blood of patients with MI**

(M ± m)

Indicator	IM, the acute period (n=60)	IM, the period of convalescence (n=60)	Control (n=20)
Leukocytes, (10^9/л)	12,7±0,8 [1,2]	6,77±0,36	5,37±0,18
Lymphocytes, (%)	57,67±2,81 [1,2]	45,65±2,32 [1]	30,1±1,75
Lymphocytes, (10^9/л)	5,74±0,65 [1,2]	3,6±0,38 [1]	2,55±0,18
$CD3^+$-cells, %	87,21±3,34 [1,2]	79,21±2,29 [1]	65,85±3,5
$CD4^+$ -cells, %	47,16±1,07 [1]	44,6±0,98	42,0±1,31
$CD8^+$-cells, %	44,16±3,78 [1]	36,6±2,7 [1]	29,4±1,9
$CD16^+$-cells, %	16,61±0,6 [1]	14,8±0,46	14,52±0,44
$CD20^+$-cells, %	18,91±0,9 [1]	16,11±0,6 [1]	13,5±0,5
$CD8^+CD28^+$-cells, %	17,6±1,1 [1]	15,5±0,9	14,8±0,6
$CD8^+CD28^-$-cells, %	5,7±0,3	5,3±0,27	5,1±0,3
$CD8^+CD28^+/CD8^+CD28^-$	3,08±0,3	2,9±0,3	2,9±0,4
$CD25^+$-cells, %	21,40±0,92 [1]	19,41±0,86 [1]	16,0±0,65
Th1 (INFγ), %	15,2±0,94 [1]	13,7±0,98	11,1±1,1
Th2 ($IL\text{-}4^+$), %	10,4±1,78	11,3±1,67	12,4±1,43
Th1/Th2	1,46±0,06 [1]	1,21±0,07	0,89±0,09

Notes: [1] is a probable difference with the control group ($p < 0.05$), [2] is the probable difference with the parameters of the convalescence period ($p < 0.05$).

Other clusters of lymphocytes tended to decrease the content compared to those at the acute period of the IM ($p > 0.05$) and did not differ with probability compared with the data of the convalescence period ($p > 0.05$). It should be noted that in this period, the probable differences with the control data had a relative content of lymphocytes of 45.65±2.32 versus 30.1±1.75% and 3.6±0.38 versus 2.55±0.18 x 10^9 ($p < 0.05$); $CD3^+$ levels were 79.21±2.29 versus 65.85±3.5% ($p < 0.05$); $CD8^+$ – 36.6±2.7 versus 29.4±1.9% ($p < 0.05$); $CD20^+$ – 16.11±0.6 versus 13.5±0.5% ($p < 0.05$) and $CD25^+$ – 19.41±0.86 versus 16.0±0.65% ($p < 0.05$).

It should be noted that in this period the distribution of the content of the indicators according to the control data was characterized by diversification, which in our opinion confirms a rather slow regression of clinical symptoms in the MI and the existence of an imbalance in both the acute period and the period of convalescence.

Conclusions

1. In patients with IM in the period of the acute period of the disease, probable violations from the cellular immunity level, characterized by an increase in the number of cells with killer activity: mature T-lymphocytes ($CD3^+$), cytotoxic T-suppressor cells ($CD8^+$), cells expressing activation marker $CD25^+$ (receptor IL-2) and a sharp drop in Th1/Th2.

2. In the period of convalescence of the IM in a greater number of patients, the prevalence of the Th2-type immune response was detected, indicating a prolonged period of convalescence and predisposition to chronic disease.

References

[1] Cen O, Longnecker R. Latent Membrane Protein 2 (LMP2). *Curr Top Microbiol Immunol*. 2015; 391: 151–80. DOI: 10.1007/978-3-319-22834-1_5

[2] Drutskaya MS, Belousov PV, Nedospasov SA. Vrozhdennoye raspoznavaniye virusov. *Molekulyarnaya biologiya*. 2011; 45 (1): 7–19. [Russian].

[3] Griffin BD, Gram AM, Mulder A, Van Leeuwen D, Claas FH, Wang F, Ressing ME, Wiertz E. EBV BILF1 evolved to downregulate cell surface display of a wide range of HLA class I molecules through their cytoplasmic tail. *J Immunology*. 2013; 190: 1672–84. DOI: 10.4049/jimmunol.1102462

[4] Fathallah I, Parroche P, Gruffat H, Zannetti C, Johansson H, Yue J, Manet E, Tommasino M, Sylla BS, Hasan UA. EBV latent membrane protein 1 is a negative regulator of TLR9. *J Immunology*. 2010; 185: 6439–47. DOI: 10.4049/jimmunol.0903459

[5] Gaudreault E, Fiola S, Olivier M, Gosselin J. Epstein-Barr virus induces MCP-1 secretion by human monocytes via TLR2. *J Virology*. 2007; 81: 8016–24. DOI: 10.1128/JVI.00403-07

[6] Fish K, Chen J, Longnecker R. Epstein-Barr virus latent membrane protein 2A enhances MYC-driven cell cycle progression in a mouse model of B lymphoma. *Blood*. 2014; 123: 530–40. doi: 10.1182/blood-2013-07-517649

[7] Fukuda M, Kawaguchi Y. Role of the immunoreceptor tyrosine-based activation motif of latent membrane protein 2A (LMP2A) in Epstein-Barr virus LMP2A-induced cell transformation. *J Virology*. 2014; 88: 5189–94. doi: 10.1128/JVI.03714-13

[8] Gibson J, Gow N, Wong SY. Expression and Funktion of innate Pattent Recognition Receptors in T and B cells. *Immun, Endoc&Metab Agents in Med Chem*. 2010; 10: 11-20.

[9] Guerreiro M, Na IK, Letsch A, Haase D, Bauer S, Meisel C, Roemhild A, Reinke P, Volk HD, Scheibenbogen C. Human peripheral blood and bone marrow EBV-specific T-cell repertoire in latent infection reveals distinct memory T-cell subsets. *Eur J Immune*. 2010; 15: 1566-76. DOI: 10.1002/eji.200940000

[10] Isakov VA, Arkhipova EI, Isakov DV. *Gerpesvirusnyye infektsii cheloveka: rukovodstvo dlya vrachey*. SPb, 2006. 303 s. [Russian].

[11] Kawai T, Akira S. The role of pattern-recognition receptors in innate immunity: update on Toll-like receptors. *Nat Immunol*. 2010; 11 (5): 373–84. DOI: 10.1038/ni.1863

[12] Krasnitskaya AS, Borovskaya NA. Immunologicheskiye aspekty khronicheskogo tonzillita, assotsiirovannogo s virus Epshteyna-Barr infektsiyey. *Fundamentalnyye issledovaniya*. 2012; 299–305. [Russian].

[13] Kudin AP. Eta «bezobidnaya» virus Epshtejna – Barr infekciya. Chast 1. Harakteristika vozbuditelya. Reakciya immunnoj sistemy na virus. *Medicinskie novosti*. 2006; 7: 25-32. [Russian].

[14] Thorley-Lawson DA, Hawkins JB, Tracy SI, Shapiro M. The pathogenesis of Epstein-Barr virus persistent infection. *Curr Opin Virol*. 2013. 3: 227–32. DOI: 10.1016/j.coviro.2013.04.005

[15] Tugizov S, Herrera R, Veluppillai P, Greenspan J, Greenspan D, Palefsky JM. Epstein-Barr Virus (EBV)-Infected Monocytes Facilitate Dissemination of EBV within the Oral Mucosal Epithelium. *J Virol*. 2007; 81 (11): 5484-96. doi: 10.1128/JVI.00171-07

[16] Vozianova ZH, Hley AI. I. Infektsiyniy mononukleoz yak polietiolohichne zakhvoryuvannya. *Suchasni infektsiyi*. 2004; 2: 37-41. [Ukrainian].

Platelet Rich Fibrin Augmented Versus Non-Augmented Glycerolized Bovine Pericardium and Polypropylene Mesh for Repairing of Large Abdominal Wall Defects

El-Husseiny, H. M.[1]

El-Maghraby, H. M.[1]

Alakraa, A. M.[1]

Kandiel, M. M. M.[2]

[1] Department of Surgery, Anesthesiology and Radiology

[2] Department of Theriogenology, Faculty of Veterinary Medicine, Benha University, PO 13736, Egypt.

Abstract

This study aimed to evaluate the use of glycerolized bovine pericardium (GBP) compared to polypropylene mesh (PPM) in repairing of large abdominal wall defects in animal model, and to investigate the role of platelet rich fibrin (PRF) in promoting this repair. Fresh bovine pericardium collected from local abattoir were processed and preserved in 99.5% glycerol. PRF matrix was harvested from fresh autologous blood (10 ml) after centrifugation. Full-thickness, mid-ventral abdominal wall defects (6 × 10 cm) were surgically created in 36 healthy goats (9 goats/group) and were repaired with an equal size of GBP, PPM, GBP-PRF, or PPM-PRF. Qualitative and gray scale quantitative ultrasonography were adopted at day 1, 1, 2, 3, 4, 8 and 12 weeks post-implantation. Three goats per group were slaughtered at 4, 8 and 12 weeks post-implantation for further gross, histopathological and tensiometric (tensile strength, load at failure and strain %) evaluations. Ultrasonography revealed significant ($P< 0.05$) improvement of implant gray scale, low subcutaneous edema and reduction of skin implant distance in PRF-augmented groups. Besides, a substantial improvement of connective tissue covering, implant incorporation, new blood vessels formation, and reduction of the inflammatory cells infiltrations were observed. Tensiometric parameters were improved in GBP-PRF group compared to the other groups. In conclusion, the obtained results not only proved the superiority of GBP over PPM, but also the advantage of PRF-augmented over non-augmented implants in treatment of large abdominal wall defects. Ultrasonographic analysis provided a satisfactory tool to evaluate the healing process of the abdominal wall defects.

Keywords: Platelet Rich Fibrin, Glycerolized Bovine Pericardium, Polypropylene mesh, Hernioplasty, Hernia.

Introduction

Surgical repair of large abdominal wall defects still becomes a significant problem and a challenge for the surgeon with recurrence being a common outcome **(1, 2)**. Prosthetic hernia repair is very important to overcome this problem **(3).**

Polypropylene mesh (PPM) has been shown to be very suitable for the repair of large abdominal wall defects in human and different animals, as it is strong and with an excellent tissue incorporation **(4)**. One of the most important drawbacks of polypropylene mesh is that it is associated with high rate of adhesion formation to the abdominal wall and underlying viscera **(4)**. This may lead to further complications as intestinal obstruction, abdominal pain, and visceral fistulation **(3 , 5).** Increased postoperative complications associated with the use of PPM has increased the attention toward the search for safe, cheap and available biodegradable prosthetic material of adequate tensile strength for repairing of large abdominal wall defects **(6)**.

As a biomaterial, pericardium has been mostly used for cardio-vascular applications, such as: arterial and vascular grafts **(7)** and artificial heart valves implantation **(8)**. It was used also, for the treatment of acquired cardiac pathologies, including post-infarction septal defects and reconstruction of mitral valve annulus or outflow obstruction **(9)**. Recently, pericardium also used for the construction of novel bio-prostheses in non-cardiac treatments such as patches for vaginal or abdominal wall defects repairing, dural defects repairing or tracheoplasty **(10)**.

Platelet Rich Fibrin (PRF) is a single fibrin membrane of immune and platelet concentrates that collects all blood components necessary for healing, immunity and minimizing postoperative inflammatory process **(11 , 12)**. PRF matrix plays a direct role in angiogenesis as it contains 6 main angiogenesis soluble factors such as fibroblast growth factor basic (FGFb), vascular endothelial growth factor (VEGF), angiopoïetin and platelet-derived growth factor (PDGF) **(13)**.

Ultrasonographic examination is an effective tool for the diagnosis of large abdominal wall defects, identification of the implants and postoperative monitoring of the subcutaneous inflammatory fluid until its complete resolution **(14 , 15)**. Quantification of the ultrasonogram by histogram analysis can enhance interpretation of good quality images through using a high-speed digital analysis system and specialized software **(16)**. They added that the ultrasonogram had 256 shades in the gray scale of the image used for quantitative assessment of the taken ultrasonograms from 0 (black / anechoic) to 255 (white / hyperechoic).

The objectives of this study are to evaluate the use of glycerolized bovine pericardium (GBP) compared to polypropylene mesh (PPM) in repairing of large abdominal wall defects in animal model, and to investigate the role of platelet rich fibrin (PRF) in enhancing this function. Moreover, to describe the application of ultrasonography in the diagnosis of large size abdominal wall defects, post-operative monitoring and quantitative gray scale histogram assessment of implanted GBP with and without PRF compared to PPM with and without PRF.

Material and methods:

Thirty-Six clinically normal and apparently healthy goats were included in this study, their ages ranged between one to three years and their weights ranged between 20 - 30 Kgs. These animals were purchased from different localities at Kalyobiya Governorate; Kept under the same circumstances, dewormed with Ivermectin 10 mg ***(Noromectin 1%, Norbrook Laboratories Limited, Northern Ireland)*** subcutaneously at a dose rate of 0.2 mg/kg b. w. and Albendazole 2.5% ***(Albendazole 2.5%, Pharma Swede Co. for pharm. Ind., Cairo. Egypt)*** orally at a dose rate of 10 mg/kg b. w. They were housed in a comfortable soft bedded stall and received water ad libitum and balanced ration of concentrate and hay. All the procedures were accomplished according to the ethics for humane treatment of animal use in research guidelines and complied with the relevant legislation of Faculty of Veterinary Medicine, Benha University, Egypt. The animals were divided into four groups (Nine goats per group).

Group 1: included animals implanted with Glycerolized Bovine Pericardium (GBP group). **Group 2**: included animals implanted with Polypropylene mesh ***(HEINE MESH, 30cm x 30cm, HEINE MEDIZIN GmbH., Dusseldorf, Germany)*** (PPM group). **Group 3** included animals implanted with Glycerolized Bovine Pericardium with Platelet Rich Fibrin (GBP-PRF group). **Group 4**: included animals implanted with Polypropylene mesh with Platelet Rich Fibrin (PPM-PRF group).

1. Pre-operative preparation

The food was withheld for 24 hours prior to surgery and the surgical site was prepared aseptically as usual. Animals were sedated using 2% Xylazine HCl ***(Xylaject, Adwia Co., Cairo, Egypt)*** in a dose rate of (0.01 mg/Kg B. wt.) and the operation seat was infiltrated using 2% lidocaine HCl ***(Debocaine, Aldebiky Co., Cairo, Egypt)***. The animals were controlled in dorsal recumbency.

2. Preparation of Glycerolized Bovine Pericardium (GBP)

Bovine Pericardial patches were processed and preserved according to the method described after **(17)**.

3. Preparation of Platelet Rich Fibrin Matrix (PRF)

PRF Matrix was prepared according to the method described by **(18)**. Specimens from PRF were obtained and fixed in 10 % buffered formal solution, stained with (H&E) stain, and examined histologically in order to detect the platelets and fibrin network.

4. Operative Technique

Full thickness, mid-ventral abdominal wall defect was created in all goats at the level of the umbilicus through 12 cm length paramedian skin incision made about 2-3 cm away from the mid line of the ventral abdominal wall. Skin was bluntly dissected away from the underlying subcutaneous tissues. The dissection was extended to expose the linea alba that was resected to create an artificial (6 x 10 cm) full thickness abdominal wall defect including the peritoneum. Hemostasis was achieved properly to control any bleeding. The prosthetic materials with suitable size proportional to the size of the defects were implanted using the intraperitoneal (Underlay) technique after **(19)**. Omentalization (Omentopexy) was created

through grasping a part of omentum that was sutured to the peripheries of the implant. The implant was sutured in position using chromic cat gut size 0 by simple interrupted suture pattern. PRF was added on the surface of the implant in PPM-PRF and GBP-PRF groups prior to skin closure. Skin incision was closed using braided silk size 1 and interrupted mattress suture pattern.

5. Post-Operative Care

Animals received an I/M course of antibiotic therapy with penicillin-streptomycin ***(Norbrook Laboratories Limited, Northern Ireland)*** at dose rate of 30.000 IU/Kg penicillin and 10 mg/Kg streptomycin for 5 days post operatively. Skin wound was daily dressed, and skin stitches were removed 14 days post operatively.

6. Post-Operative follow up and evaluation

The animals were kept under observation to detect any changes or complications and they were evaluated depending on ultrasonographic examination at day 1, 1, 2, 3, 4, 8 and 12 weeks post-implantation: Three goats from each group were slaughtered at 4, 8 and 12 weeks post operatively for further evaluations depending on gross pathological and histopathological examinations. Tensiometric evaluations were adopted at 8 and 12 weeks post operatively.

6.1. Ultrasonographic Evaluation

Ultrasonographic Examination was performed using a portable ultrasound machine ***(Eickemyer, Magic 1500, Co., Ltd, UK)*** with adjusted 5 MHz linear array transducer. The machine was set at 4.6 cm depth and 52 gain. prior to ultrasonographic examination. The animals were ultrasonographically examined according to **(14).** Quantitative assessment of implant gray scale (IGS), subcutaneous gray scale (SGS) and skin implant distance (SID) were achieved by image brightness analysis [on gray scale units from 0 (black) to 255 (white)] by using dedicated software Image J ***(NACL Co. Ltd., Tokyo, Japan)*** to obtain the mean gray value of the analyzed ultrasonographic image.

6.2. Tensiometric Evaluation

Transverse strips (4 cm width and 10 cm length) harvested from the implanted grafts after slaughtering at 8 and 12 weeks post operatively. These strips included the implanted prosthetic materials and bilateral adjacent body wall. Specimens were collected in containers of normal saline, transported to the laboratory in icebox, and the biomechanical testing was done within 3 hours of samples collection. They were mounted into the grips for computer controlled mechanical testing using tensile strength testing apparatus (***Servo Universal Testing Machine, WAW-600, Beijing Sinofound Co., Ltd, China***). The clamps of tensometer were coated from inside by a piece of felt and tightened to avoid slipping of tissue specimens, then proximal and distal parts of specimens were secured on the two metal clamps of the tensometer. All specimens were loaded and elongated till failure at speed of 50 mm/min. Tensile strength (TS), Load at failure (LF) and Strain percent were recorded according to **(2).**

6.3. Macroscopic Examination

Gross evaluation of the implantation site was conducted after slaughtering of the animals at 4, 8 and 12 weeks post operatively post operatively. A rectangular 6 cm in width skin area was removed and the parietal surface of the implant was examined to detect the connective tissue covering. The implant was excised and reflected to examine the visceral surface to record the neovascularization, connective tissue covering and degree of adhesion. The numerical scores of adhesions ranged from 0 to 4 were evaluated according to Modified Hopkins adhesion score **(Table 1)** performed by **(20)**.

6.4. Microscopic Examination

Specimens were collected from patch grafts after slaughtering of the animals in different groups at 4, 8 and 12 weeks following implantation, fixed in 10% formal saline for 24 hours for preparation of paraffin sections. Thin sections of 4 microns thickness were cut and stained with Hematoxylin and Eosin stain (H & E) for examination through the light electric microscope **(21)**.

6.5. Statistical Analysis

The obtained results were tabulated and expressed as Mean ± Standard Error of Means (SEM). All statistical analyses were conducted by using IBM-SPSS (Ver. 23). For comparison of the data of different groups at the same time points after surgery, the obtained data were compared using One Way Analysis of Variance (ANOVA) and post-hoc with Duncan multiple comparison test. For comparison of the data of the same group with the pre-surgical values, data were analyzed

using One Way ANOVA and post-hoc with Dunnett multiple comparison procedure. In order to compare the data of two time points (8 weeks versus 12 weeks), independent student t-test was conducted.

Results

I. Ultrasonographic Examination

I.1. Qualitative ultrasonographic assessment

On B-scan, the implanted materials in different groups appeared as thin white hyperechoic lines surrounded by anechoic area representing the acute inflammatory fluid at first day post implantation.

In PRF augmented groups, PRF appeared as a small hypoechogenic area surrounding the implants.

There was gradual increase in the echogenicity of the prosthetic implants during the 1st, 2nd and 3rd weeks post implantation. This was highly marked in PRF groups that also showed incomplete infilling of the implants with multiple hypoechogenic dots representing the newly formed connective tissue at 3rd week post implantation. In PPM group, the echogenicity of the prosthetic implants revealed incomplete infilling of the implants with few hypoechogenic dots.

Subcutaneous fluid appeared as anechoic area surrounding the prosthetic implants in different groups at 1st week post implantation. It was markedly increase in GBP group, while in PPM group it was lower and in PPM-PRF and GBP-PRF group it was the lowest. At 2nd week post implantation, it showed increase in GBP group, while in PPM group it showed gradual resolution with presence of few hypoechogenic dots, but in PPM-PRF and GBP-PRF groups it showed complete resolution with presence of multiple hypoechogenic dots representing the newly formed connective tissue. At 3rd week post implantation, subcutaneous fluid showed gradual resolution in GBP group. Subcutaneous fluid showed complete resolution in GBP and PPM groups at 4th week post implantation.

At 8th and 12th weeks, ultrasonographic image of subcutaneous area revealed gradual increase in the echogenicity in different groups that revealed presence of multiple hypoechogenic to few hyperechogenic dots in subcutaneous area in non-PRF groups, while in PRF groups it revealed presence of multiple hyperechogenic dots in the subcutaneous area surrounding the implants **(Fig. 1).**

I.2.Quantitative ultrasonographic assessment

I.2.a. Implant Gray Scale (IGS)

The mean IGS within each group showed significant ($p < 0.001$) difference at different time points of the study. The recorded IGS means of all groups were tabulated in Table 3. Comparing between different groups verified that the mean IGS of non-PRF groups was significant ($p < 0.001$) higher than PRF groups at the 1st day post implantation, while that of PRF groups was significant ($p < 0.001$) higher than that of non-PRF groups at 1st and 2nd weeks post implantation. At 4th and 8th weeks post implantation, the mean IGS of GBP-PRF group was significantly ($p < 0.01$) higher than that of the other groups and still significant ($p < 0.001$) higher than other groups at 12th week post implantation. Moreover, the mean IGS of PPM-PRF group was significant ($p < 0.01$) higher than that of the other groups at 2nd week post implantation. **(Table 2 & Fig. 1)**.

I.2.b. Subcutaneous Gray Scale (SGS)

The mean SGS within each group showed significant ($p < 0.001$) difference at different time points of the study. The recorded subcutaneous gray scale means (SGS) of all groups were tabulated in Table 4. Comparing between different groups showed that the mean SGS of GBP and GBP-PRF groups was significant ($p < 0.001$) lower than PPM and PPM-PRF groups at the 1st day post implantation, but it was significantly ($p < 0.01$) higher in PRF groups than in non-PRF groups at 1st week post implantation. The mean SGS of PPM-PRF group was significant ($p < 0.001$) higher than the other groups at 2nd, 3rd, 4th and 8th weeks post implantation. At 12th week after implantation, the mean SGS of GBP group was significantly ($p < 0.001$) lower than that of the other groups **(Table 3 & Fig. 1)**.

I.2.c. Skin Implant Distance (SID) [mm]

The recorded skin implant distance (SID) means of all groups were tabulated in Table 5. The mean SID of GBP and GBP-PRF groups was significant ($p < 0.05$) higher than that of PPM and PPM-PRF groups at the 1st day post implantation. The mean SID of GBP group was significant ($p < 0.005$) higher than that of the other groups at 1st, 2nd, 3rd and 4th weeks post implantation. Moreover, it was still significantly ($p < 0.05$) higher than the other groups at 12th week post implantation **(Table 4)**.

II. Tensiometric Evaluation

The site of breakage (failure) of the tested specimens was either at the interface between implant and muscle or on the muscle itself at one end of the implant.

Tensiometric characters showed changes over time points of the experiment. Comparison between different groups showed that the mean of both tensile strength and load at failure of GBP-PRF and PPM-PRF groups was very highly significant ($p < 0.001$) at 8 weeks and extreme highly significant ($p < 0.0001$) at 12 weeks higher than that of GBP and PPM groups post implantation. **(Tables 5 &6 and Fig. 2)**.

The mean strain % showed no significant change between different groups at 8 weeks post implantation. The mean strain % of GBP and GBP-PRF groups tend to be significant ($p = 0.065$) higher than that of PPM-PRF group at the 12 weeks post implantation **(Table 7 & Fig. 2)**.

III. Macroscopic Examination

At 4th week post operatively, the parietal surface of different implanted materials was covered by a thin layer of fibrous connective tissue with good incorporation of the implants with the recipient abdominal wall. In GBP-PRF and PPM-PRF groups, outer thin neovascularization was observed**.** The connective tissue covering, and neovascularization increased gradually at 8th and 12th weeks post operatively and became more prominent in GBP-PRF and PPM-PRF than GBP and PPM groups**.** The borders of the implanted material at PPM group showed folding and irregularities that were absent in the other groups **(Fig. 3).**

Macroscopic examination of the visceral surface of the implanted materials at 4th week post operatively revealed that they were encapsulated with fibrous connective tissue which increased gradually at 8th and 12th months post operatively and became more prominent in GBP-PRF and PPM-PRF than GBP and PPM groups **(Fig. 4).**

The degree of adhesion was more severe in PPM group than the others, but it was the mildest in GBP-PRF group. The adhesion score 0 (no adhesion) was recorded only in GBP-PRF and PPM-PRF groups. Score 3 was recorded in GBP and PPM groups, while score 4 was recorded only in PPM group where severe matted adhesion between the PPM and the intestines was observed and causing unavoidable serosal damage on dissection. Scores (3) and (4) were absent only in PRF augmented groups **(Table 8 & Fig. 5).**

IV. Microscopic Examination

Histological examination of native unprocessed bovine pericardium revealed its intact normal structure composed of a single layer of simple squamous epithelium and connective tissue mainly elastin and collagen. Collagen fibers were more abundant, with marked organization at different levels range from fibrils to laminates and fibers. The collagen appeared red with clear flattened fibroblasts containing peripheral nuclei. Microscopic picture of glycerolized bovine pericardium (GBP) revealed absence of the epithelial layer and presence only of few necrotic nuclei with the collagen fibers that appeared red in color. PRF appeared histologically as dense, mature, homogenous and well-organized light pink fibrin network with presence of blood platelets aggregates that were discoidal, red and non-nucleated cells **(Fig. 6)**.

At 4th week after implantation, histological examination of GBP group showed normal intact histological structure of GBP formed of dense collagen fibers surrounded by few numbers of inflammatory cells infiltration. In PPM group, the inflammatory cells were widely scattered around mesh fibers. In PRF-augmented groups, there were focal areas of few numbers of inflammatory cells. The granulation tissue formation was observed in the form of newly formed loose fibrous tissue and few scattered round fibroblasts surrounded by thin collagen fibers. These fibers were more abundant in GBP group, immature in PPM group and more pronounced parallel collagen fibers with presence of fibroblastic cells appeared round to ovoid in shape in PRF-augmented groups.

At 8th week, the inflammatory cells were severely reduced and observed as focal areas of few inflammatory cells in Non PRF-augmented groups. They were completely reduced in PRF-augmented groups. The loose connective tissue was gradually changed to dense fibrous connective tissue with presence of round to ovoid fibroblasts in non PRF-augmented groups. Wide areas of dense and parallel oriented collagen proliferations were observed with presence of multiple ovoid fibroblasts surrounding the collagen fibers in PRF-augmented groups. The neovascularization started to appear within the fibrous tissue in PRF-augmented groups.

At 12th week, there was small focal areas of very few inflammatory cells aggregations in GBP group and they were mainly around mesh fibers in PPM group. The inflammatory cells were completely absent in PRF-augmented groups. Granulation

tissue formation was observed by presence of dense fibrous connective tissue formed mainly of collagen fibers with presence of spindle shape fibroblasts in non PRF-augmented groups. In PRF-augmented groups, there were fibroblastic cells and collagen proliferations. Collagen became denser, abundant and surrounding the multiple spindle shape fibroblasts that observed more elongated, with flattened nuclei. Neovascularization were observed within the fibrous tissue of non-PRF groups. Presence of multiple newly formed blood capillaries and vessels with their characteristic endothelial lining within the fibrous tissue in PRF-augmented groups **(Fig. 7)**.

Discussion

Processing and preservation of bovine pericardium using glycerol was an efficient method for pericardial treatment and decellularization. Glycerolized bovine pericardium (GBP) was superior to lyophilized (freeze-dried) bovine pericardium in treatment of large abdominal wall defects **(22)**. Results of the present study revealed that GBP was compatible and acceptable by the recipient tissue for long periods after implantation. This was attributed to successive decellularization of bovine pericardial tissue that leaves only the collagenous structure of extra-cellular matrix (ECM) that is common (non - antigenic) in different domestic animals **(23)**. In our study, GBP implants showed less intense post implantation inflammatory reaction compared to PPM, this comes in line with that mentioned by **(2 , 22)**.

Size of abdominal wall defect (6 x 10) cm created in goats when compared to the animal size is considered large and representative of large abdominal defects encountered in different large animals that require bridging of these large defects using prosthetic implants. This finding comes in line with **(24)**.

In the present study, ultrasonographic examination of GBP and PPM groups at 1st week following implantation revealed presence of anechoic image representing inflammatory fluid surrounding the hyperechoic implants that was more obvious in GBP group than PPM group. Complete resolution of this fluid noticed at 2nd week post implantation in all groups. These findings were attributed to inadequate hemostasis or rough excessive dissection during defect repair **(25)**. Sonogram of PRF-augmented groups at 1st week following implantation revealed presence of slight anechoic fluid surrounding the hyperechoic implant. This finding confirmed the anti-inflammatory effect of PRF **(26)**. At 2nd, 3rd and 4th weeks following implantation, sonography of GBP and PPM groups showed gradual and slight improvement of echogenicity that was more obvious in GBP group. At 8th and 12th weeks, results revealed gradual filling of the defects by echogenic dots representing collagen fibers which was incomplete infilling of PPM pores with collagen fibers. These findings agree with **(25)**. Ultrasonographic examination of PRF-augmented groups at 2nd, 3rd and 4th weeks following implantation revealed presence gradual but quick improvement of the echogenicity that was more obvious at 8th and 12th weeks following implantation and showed complete filling of the defects with hyperechoic dots. This occurred because PRF matrix enhances the healing and covering of the injured tissues as they affect the metabolism of epithelial cells and fibroblasts and enable them to extend toward and cover the wound faster **(13)**.

Quantitative ultrasonographic assessment of implants in different groups showed that implant and subcutaneous gray scale were significant ($p < 0.05$) higher in PRF-augmented groups at different time points of the study. Seven different growth factors and cytokines are released from degranulation of PRF and have a necessary role in stimulation of the healing of soft and hard tissues **(12)**. The quantitative assessment also showed that skin implant distance was significant ($p < 0.05$) lower in PRF-augmented groups at different time points of the study. PRF composed of platelet concentrates that collect all blood components have the ability to regulate the inflammatory process **(11 , 12)**.

Tensiometric evaluation of different groups revealed that the site of breakage (failure) of all tested implant strips was between the implant and surrounding rectus muscles (implant -muscle interface). The tensile strength of the rectus muscles and the newly formed fascia is lower than that at the implant site **(2)**. There was no significant ($p < 0.05$) change in the mean tensile strength and load at failure in GBP and PPM groups at 8th and 12th weeks post implantation. Both GBP and PPM were strong enough to keep the integrity of abdominal wall **(2 , 17 & 22)**. The mean tensile strength and load at failure of PRF-augmented groups were significant ($p < 0.05$) higher than those of GBP and PPM at 8th and 12th weeks post implantation. This finding comes in line with **(27)**. The mean tensile strength and load at failure of all tested groups showed significant ($p < 0.05$) increase at the 12th week higher than that at the 8th week post implantation. The abdominal wall becomes stronger during the late periods after implantation due to formation of new tissue around the implant **(2)**. The mean strain (%) showed no significant ($p < 0.05$) change between different tested groups at 8th week following implantation. This coincides with **(28)** who recorded that there was no significant difference in strain between different graft types over time that reached 52 weeks.

Macroscopic picture of different implants showed that connective tissue covering and neovascularization were more prominent and gradually increased by time in GBP group than PPM group and this finding agrees with **(2)**. Adhesion scores

were higher and more intense in PPM group than GBP group as repairing of abdominal wall defects using PPM usually results in severe degrees of adhesions with the visceral organs that results in more complications as intestinal fistula **(29)** moreover, GBP could be used for repairing of abdominal wall defects without stimulating adhesions with underlying viscera as the adhesion only recorded between the peritoneal surface of GBP and the omentum and this was attributed this to ischemia or foreign bodies that may encountered during the implantation **(17)**. Adhesion scores were lower in PRF-augmented groups and score 0 was recorded only in them. Using of PRP can result in reduction of adhesion occurrence and degree **(30)** and this is due to the anti-inflammatory characters of platelet rich concentrates **(26)**.

Microscopic examination of unprocessed bovine pericardium revealed that it is composed of a single layer of lining epithelial cells (simple squamous epithelium) and connective tissue mainly elastin and collagen. The antigenicity of unprocessed bovine pericardium as a xenograft was attributed to its cellular structure **(32)**. Histology of GBP revealed its a cellular structure with absence of the epithelial layer and presence only of few necrotic nuclei with the collagen biomatrix (ECM). This finding agrees with **(23)** who mentioned that, histological examination is very important to assess the efficacy of pericardial decellularization. Histopathological examination of PRF showed presence of dense, mature, homogenous and well-organized fibrin network with aggregates of blood platelets that appeared discoidal, red non-nucleated cells in color **(31)**. Microscopic examination of GBP and PPM groups showed that inflammatory cells infiltration was lower in GBP group than PPM group and revealed its gradual decrease of it by time. These findings come in agreement with **(2)**. Inflammatory cells infiltration was lower in PRF-augmented groups at 4th, 8th and 12th weeks following implantation. This finding coincides with **(26)** who attributed this result to the anti-inflammatory properties of platelet rich concentrates. Newly formed connective tissue was more abundant in GBP group than PPM group which was gradually increased by time. This comes in agreement with **(2).** It was more prominent, obvious, regular and abundant in PRF-augmented groups at 4th, 8th and 12th weeks following implantation. Platelet cytokines and growth promoters have the ability to propagate and improve the healing process, enhance cell proliferation and differentiation because of their capacity to stimulate cell migration and proliferation (specially by PDGFs) and induce fibrin matrix remodeling as well as secretion of a cicatricial collagen matrix (specially by TGF- β) **(27)**. Neovascularization was more obvious in PRF-augmented groups at 8th week following implantation and increased in number and size at 12th week following implantation. PRF matrix plays a direct role in angiogenesis as it contains 6 main angiogenesis soluble factors such as fibroblast growth factor basic (FGFb), vascular endothelial growth factor (VEGF), angiopoïetin and platelet-derived growth factor (PDGF) **(13)**.

Conclusion

The results proved the priority of Glycerolized Bovine Pericardium (GBP) and Platelet Rich Fibrin (PRF) augmented implants in treatment of large abdominal wall defects. PRF provided favorable results in enhancement of the healing process through enhancing neovascularization, increasing tissue deposition and incorporation., reducing postoperative inflammatory reaction and minimizing the post-operative complications such as adhesions and recurrences.

Ultrasonographic examinations using histogram gray scale analysis provided a satisfactory tool to post operatively evaluate the healing process of abdominal wall defects repaired using different prosthetic implants.

Conflict of interest

The authors have no conflict of interest to declare.

References

[1] Abouelnasr, K. S., Zaghloul, A. E. and Karrouf, G. I. (2014): Comparative evaluation of glycerolized bovine pericardium implant with prolene mesh for closure of large abdominal wall defects in dogs. IJVR, 15 (3): 211-217.

[2] AL-Asadi, R. N. and Hummadi, S. K. (2011): Ultrasonographic Evaluation of Hernioplasty of Experimentally Induced Large Ventro-lateral Hernia in Bucks. The Iraqi J. Vet. Med. 35 (2): 105- 112.

[3] Badylak, S. F. (2007): The extracellular matrix as a biologic scaffold material. Biomaterials. 28: 3587-3593.

[4] Banchroft, J. D.; Stevens, A. L. and Turner, D. R. (1996): Theory and practice of histological technique. 4th Ed., London, New York, Churchill Livingstone, San Francisco, Tokyo. Pp. 210-250.

[5] Baptista, M. L.; Bonsack, M. S. and Delaney, J. P. (2000). Seprafilm reduces adhesions to polypropylene mesh. Surgery. 128: 86-92.

[6] Bellon, J. M., Conteras, L. A., Pascual, G., and Bunjan, J. (2000): Evaluation of the Acute scarring response to the implant of different types of biomaterial in the abdominal wall. J Mat Sc: Materials in the Medicine; 11(1): 25-9.

[7] Choukroun, J., Diss, A. and Simonpieri, A. (2006): Platelet-rich fibrin (PRF): a second-generation platelet concentrate. Part V: histologic evaluations of PRF effects on bone allograft maturation in sinus lift. Oral Surg. Oral Med. Oral Pathol. Oral Radiol. Endodont. 101: 299–303.

[8] Dohan, D. M., Choukroun, J., Diss, A., Dohan, S. L., Dohan, A. J. J., Mouhyi, J. and Bruno Gogly (2006) B: Platelet-rich fibrin (PRF): A second-generation platelet concentrate. Part III: Leucocyte activation: A new feature for platelet concentrates? Oral Surg Oral Med Oral Pathol Oral Radiol Endod. 10: 51-55.

[9] Dohan, D. M., Choukroun, J., Diss, A., Dohan, S. L., Dohan, A. J. J., Mouhyi, J. and Bruno Gogly (2006) A: Platelet-rich fibrin (PRF): A second-generation platelet concentrate. Part I: Technological concepts and evolution. Oral Surg Oral Med Oral Pathol Oral Radiol Endod. 101: 37–44.

[10] Dubcenco, E., Assumpcao, L., Dray, X., Gabrielson, K., Ruben, D., Pipitone, L., Donatelli., Krishnamurthy, D., Baker, J. and Marohn, M. (2009). Adhesion formation after peritoneoscopy with liver biopsy in a survival porcine model: comparison of laparotomy, laparoscopy, and transgastric natural orifice transluminal endoscopic surgery (NOTES). Endoscopy Journal; 41(11): 971 – 978.

[11] Eryilamz, R.; Sahin, M. and Tekeliogu, M. H. (2006): Which repair in umbilical hernia of adult primary or mesh. Int Surg. 91: 258-261.

[12] Escande Remi; Nizar Khelil; Isabelle Di Centa; Caroline Roques; Maguette Ba; Fatima Medjahed-Hamidi; Frederic Chaubet; Didier Letourneur; Emmanuel Lansac and Anne Meddahi-Pelle (2011): Pericardial Processing: Challenges, Outcomes and Future Prospects, Biomaterials Science and Engineering: 437-456.

[13] Hafeez, Y. M., Zuki, A. Z., Logman, M. Y., Noordin, M. M. and Yusof, N. (2005): Comparative evaluation of the processed bovine tunica vaginalis implant in a rat model. Anat. Sci. Int. 80: 181-188.

[14] Hafeez, Y. M., Zuki, A. Z., Logman, M. Y., Yusof, N., Asnah, H. and Noordin, M. M. (2004): Glycerol preserved bovine pericardium for abdominal wall reconstruction: experimental study in rat model. Med. J. Malaysia. 59: 117-118.

[15] James, N. L., Poole-Warren, L. A, Schindhelm, K., Milthorpe, B. K., Mitchell, R. M., Mitchell, R. E., and Howlett, C. R. (1991): Comparative evaluation of treated bovine pericardium as a xenograft for hernia repair. Biomaterials 12: 801-807.

[16] Kader, N. H., Abass, B. T. and Al-Sadi, H. I. (2005): A comparative experimental study of the use of tunica vaginalis and pericardium as allografts for hernioplasty in sheep. Iraqi J. Vet. Sci., 19: 57-70.

[17] Kassem, M. M., El-Kammar, M. H., Korittum, A. S. and Abdel-Wahed, A. A. (2014): Using of Polypropylene Mesh for Hernioplasty in Calves Alexandria Journal of Veterinary Sciences, 40: 112-117.

[18] Kumar, A., Mohindroo, J., Sangwan, V., Mahajan, S. K., Singh, K., Anand, A. And Saini, N. S. (2014): Ultrasonographic evaluation of massive abdominal wall swellings in cattle and buffaloes. Turkish Journal of Veterinary and Animal Sciences. 38: 100-103.

[19] Kumar, N., Mathew, D. D., Gangwar, A. K., Remya, V., Muthalavi, M. A., Maiti, S. K., Sharma, A. K. (2014): Reconstruction of large ventrolateral hernia in a buffalo with acellular dermal matrix: a method for treating large hernias in animals. Vet. arhiv 84: 691-699.

[20] Manzoor Dar, Tajamul Hakim, Ajaz Shah, Latief Najar, Gowhar Yaqoob, Faiqah Lanker. (2016): Use of autologous platelet-rich fibrin in osseous regeneration after cystic enucleation: A clinical study; Journal of Oral Biology and Craniofacial Research. 227-230.

[21] Marmotti, A., Rossi, R., Castoldi, F., Roveda, E., Michielon, G. and Peretti, G. M. (2015): PRP and articular cartilage: a clinical update. Bio Med. Res. Int. 4 (2): 215-221.

[22] Matthews, B. D., Pratt, B. L., Pollinger, H. S., Backus, C. L., Kercher, K. W., Sing, R. F. and Heniford, B. T. (2003): Assessment of adhesion formation to intra-abdominal polypropylene mesh and polytetrafluoroethylene mesh. J. Surg. Res. 114 (2): 126-132.

[23] Mustafa Tunali, Hakan Özdemir, Zafer Küçükodacı, Serhan Akman, Elif Öncü, Mustafa Aydınbelge, Melek Akman and Erhan Firatli (2016): A New Centrifugation Method for the Improvement of Platelet- Rich Fibrin Products: A preliminary Study. British Journal of Medicine and Medical Research. 13 (6): 1-10.

[24] Schmidt, C. E. and Baier, J. M. (2000): Acellular vascular tissues: natural biomaterials for tissue repair and tissue engineering. Biomaterials, 21 (22): 2215–2231.

[25] Schoen, F. J. and Levy, R. J. (1999): Tissue heart valves: current challenges and future research perspectives. J Biomed Mater Res, 47 (4): 439–465.

[26] Shoukry, M., El-Keley, M., Hamouda, M. and Gadallah, S. (1997): Commercial polyester fabric repair of abdominal hernias and defects. Vet. Rec. 140: 606-607.

[27] Sommers, K. E. and David, T. E. (1997): Aortic valve replacement with patch enlargement of the aortic annulus. Ann Thorac Surg, Vol. 63 (6): 1608-1612.

[28] Takamura, M., Yasuda, T., Nakano, A. Shima, H. and Neo, M. (2017): The effect of platelet-rich plasma on Achilles tendon he 448 a ling in a rabbit model. Acta. Orthop. Traumatol. Turc.: 65–72.
[29] Tsukiyama, K., Jezie, A., Acorda, Magr and Haruo yamada. (1996): Evaluation of Superficial Digital Flexor Tendinitis in Racing Horses Through Gray Scale Histogram Analysis of Tendon Ultrasonograms. Veterinary Radiology & Ultrasound, 37 (1): 46-50.
[30] Van der Velden, M.A. and Klein, W.R. (1994): A modified technique for implantation of polypropylene mesh for the repair of external abdominal hernias in horses: a review of 21 cases. Vet. Quart. 16, Suppl. 2, S108-S110.
[31] Van Eps, J., Fernandez-Moure, J., Cabrera, F., Wang, X., Karim, A., Corradetti, B., Tasciotti, E. and Weiner, B. (2016): Decreased hernia recurrence using autologous platelet-rich plasma (PRP) with Strattice™ mesh in a rodent ventral hernia model. Surg. Endosc.: 3239 – 3249.
[32] Vilar, J. M., CORBERA, J. A. and Giuseppe Spinella. (2011): Double-layer mesh hernioplasty for repairing umbilical hernias in 10 goats. Turk. J. Vet. Anim. Sci. 35 (2): 131-135.

Tables:

Table (1): Modified Hopkins adhesion score, adapted by **Dubcenco, et. al., (2009).**

Table (2): Changes in Implant Gray Scale (IGS) Values in the Different Groups after Implantation.

Table (3): Changes in Subcutaneous Gray Scale (SGS) Values in the Different Groups after implantation.

Table (4): Changes in Skin Implant Distance (SID) Values in the Different Groups after Implantation.

Table (5): Changes in Tensile Strength in the Different Groups at 8th and 12th weeks after implantation.

Table (6): Changes in Load at Failure Values in the Different Groups at 8th and 12th weeks after implantation.

Table (7): Changes in Strain (%) Values in the Different Groups at 2nd and 3rd months after implantation.

Table (8): Adhesion score in Different Tested Groups according to Modified Hopkins Adhesion Score.

Tables footnotes

Table (2): Data was presented as mean ± Standard Error (SE). Values with different superscript numbers within the same column were significantly different at $p < 0.001$. Data with different superscript letters within the same row were significantly different at $p < 0.001$ and $p < 0.0001$.

Table (3): Data was presented as mean ± Standard Error (SE). Values with different superscript numbers within the same column were significantly different at $p < 0.001$. Data with different superscript letters within the same row were significantly different at $p < 0.001$ and $p < 0.0001$.

Table (4): Data was presented as mean ± Standard Error (SE). Values with different superscript numbers within the same column were significantly different at $p < 0.001$. Data with different superscript letters within the same row were significantly different at $p < 0.001$ and $p < 0.0001$.

Table (5): Data was presented as mean ± Standard Error (SE). Values with different superscript letters within the same column were significantly different $p < 0.001$ at 8th week and $p < 0.0001$ at 12th week.

Table (6): Data was presented as mean ± Standard Error (SE). Values with different superscript letters within the same column were significantly different $p < 0.001$ at 8th week and $p < 0.0001$ at 12th week.

Table (7): Data was presented as mean ± Standard Error (SE). Values with different superscript letters within the same column were significantly different at $p = 0.065$ at 12th week.

Legends of Figures:

Figure (1): Qualitative and quantitative ultrasonographic assessment of the prosthetic implants in different groups at 1st day, 1st, 2nd, 3rd, 4th, 8th and 12th weeks post implantation. Qualitative ultrasonogram (a), implant gray scale (b) and subcutaneous gray scale.

Figure (2): Tensiometric characters of the prosthetic implants in different groups at 8th and 12th weeks post implantation. Site of breakage or failure (white arrow).

Figure (3): Macroscopic picture of the parietal surface of the prosthetic implants in different groups at 4th, 8th and 12th weeks post implantation. Newly formed blood vessels (White arrows).

Figure (4): Macroscopic picture of the visceral surface of the prosthetic implants in different groups at 4th, 8th and 12th weeks post implantation. Newly formed blood vessels (White arrows).

Figure (5): Adhesion Score in different groups according to Modified Hopkins Adhesion Score. Score 0 with no adhesion (A), Score 1 with single filmy adhesion between the implant and the viscera (B), Score 2 with multiple filmy adhesions between the implant and the viscera (C), Score 3 with dense adhesions between the implant and the viscera (D), Score 4 with matted adhesions between the implant and the viscera (E).

Figure (6): Microscopic picture of native unprocessed bovine pericardium (A), Glycerolized Bovine Pericardium (GBP) (B) and Platelet Rich Fibrin (PRF). Single epithelial layer (Epi, red arrows), different levels of collagen organization (C, blue arrows), the fibroblasts (black arrows), few necrotic nuclei (yellow arrows), fibrin network (n), aggregates of blood platelets (white arrows). (H&E x40)

Figure (7): Microscopic picture of the prosthetic implants in different groups at 4th, 8th and 12th weeks post implantation. Intact structure of pericardial implant (yellow arrows), inflammatory cells infiltrations (green arrows), newly formed connective tissue (black arrows), neovascularization (blue arrows), elongated spindle shape fibroblasts surrounding collagen fibers (red arrows). (H&E x16)

Score	Frequency	Size/width (cm)	Density	Dissection
0	0	No adhesion	No adhesion	No adhesion
1	1	< 1	Single thin, filmy adhesion	Minimal blunt dissection, tears easily
2	1-2	1-2	Multiple thin, filmy adhesions	Blunt dissection only
3	3-4	2-3	Dense adhesion(s) with or without filmy adhesions	Sharp dissection or electrocautery, no organ/serosal damage
4	4+	3+	Matted adhesion(s) with or without filmy adhesions	Sharp dissection or electrocautery, with unavoidable organ/serosal damage

Time	GBP Group	PPM Group	GBP-PRF Group	PPM-PRF Group
Day 1	$145.34 \pm 2.13^{b\,1}$	$166.59 \pm 2.64^{a\,1}$	$137.39 \pm 2.23^{c\,2}$	$107.44 \pm 1.72^{d\,2\,3}$
Week 1	$70.15 \pm 3.39^{b\,4}$	$46.04 \pm 3.06^{c\,6}$	$90.50 \pm 4.85^{a\,4}$	$100.73 \pm 0.58^{a\,3}$
Week 2	$88.24 \pm 5.88^{b\,3}$	$75.17 \pm 2.34^{c\,5}$	$94.91 \pm 1.67^{a\,b\,3\,4}$	$103.40 \pm 4.28^{a\,2\,3}$
Week 3	$93.26 \pm 2.77^{b\,2\,3}$	$89.03 \pm 1.62^{b\,4}$	$114.49 \pm 2.65^{a\,3}$	$111.72 \pm 0.80^{a\,2\,3}$
Week 4	$108.63 \pm 11.93^{a\,b\,2}$	$97.31 \pm 3.50^{a\,3}$	$136.52 \pm 10.83^{a\,2}$	$114.40 \pm 4.37^{a\,b\,2}$
Week 8	$128.33 \pm 6.31^{b\,1}$	$105.57 \pm 1.47^{c\,2}$	$166.23 \pm 1.68^{a\,1}$	$129.00 \pm 1.08^{b\,1}$
Week 12	$135.49 \pm 1.93^{b\,1}$	$112.22 \pm 2.42^{b\,2}$	$177.88 \pm 12.88^{a\,1}$	$129.56 \pm 6.98^{b\,1}$

Time	GBP Group	PPM Group	GBP-PRF Group	PPM-PRF Group
Day 1	$68.95 \pm 3.68^{b\,1}$	$110.33 \pm 6.77^{a\,1}$	$54.32 \pm 2.33^{b\,4}$	$97.64 \pm 6.77^{a\,1}$
Week 1	$16.42 \pm 0.56^{b\,3}$	$38.77 \pm 0.65^{a\,5}$	$35.25 \pm 3.13^{a\,5}$	$53.43 \pm 10.21^{a\,3}$
Week 2	$17.21 \pm 0.99^{c\,3}$	$41.91 \pm 1.57^{b\,5}$	$41.93 \pm 2.68^{b\,5}$	$75.44 \pm 9.39^{a\,2}$
Week 3	$19.40 \pm 1.07^{c\,3}$	$49.12 \pm 3.04^{b\,5}$	$60.27 \pm 5.46^{b\,3\,4}$	$85.82 \pm 1.10^{a\,1\,2}$
Week 4	$22.46 \pm 2.05^{d\,3}$	$60.26 \pm 2.18^{b\,4}$	$67.69 \pm 4.33^{b\,2\,3}$	$94.19 \pm 5.94^{a\,1\,2}$

Week 8	40.90 ± 1.75 d 2	82.54 ± 2.19 b 3	71.11 ± 1.13 c 2	97.41 ± 2.46 a 1
Week 12	64.18 ± 6.15 b 1	98.62 ± 3.43 a 2	99.53 ± 2.06 a 1	104.42 ± 3.44 a 1

Time	GBP Group	PPM Group	GBP-PRF Group	PPM-PRF Group
Day 1	4.00 ± 0.40 a 4	1.17 ± 0.09 c 4	5.00 ± 0.58 a 3 4	2.58 ± 0.36 b 2 3 4
Week 1	18.00 ± 1.15 a 1	4.73 ± 0.29 c 1	9.08 ± 0.30 b 1	4.00 ± 0.29 c 1
Week 2	16.83 ± 0.93 a 1	4.13 ± 0.18 c 2	8.50 ± 0.29 b 1	3.00 ± 0.14 c 2
Week 3	15.50 ± 0.76 a 1	3.83 ± 0.12 c 2	6.50 ± 0.29 b 2	2.75 ± 0.14 c 2 3
Week 4	15.33 ± 0.88 a 1	3.23 ± 0.12 c 3	5.90 ± 0.06 b 2 3	2.68 ± 0.09 c 2 3
Week 8	11.00 ± 0.58 a 2	3.03 ± 0.09 c 3	5.13 ± 0.09 b 3 4	2.20 ± 0.12 c 3 4
Week 12	7.33 ± 1.45 a 3	2.77 ± 0.15 b 3	4.50 ± 0.29 b 4	1.97 ± 0.20 b 4

Time	Week 8	Week 12
GBP Group	19.27 ± 0.43 b	26.13 ± 0.47 b
PPM Group	20.67 ± 1.20b	26.33 ± 0.88 b
GBP-PRF Group	27.20 ± 1.42a	33.10 ± 0.83 a
PPM-PRF Group	28.33 ± 0.88a	34.03 ± 1.28 a

Time	Week 8	Week 12
GBP Group	83.80 ± 0.92 b	96.87 ± 0.86 b
PPM Group	85.77 ± 1.69b	97.57 ± 0.87 b
GBP-PRF Group	93.67 ± 1.45 a	102.43 ± 2.31 a
PPM-PRF Group	96.10 ± 2.28 a	104.67 ± 0.88 a

Time	Week 8	Week 12
GBP Group	41.83 ± 1.98	47.67 ± 1.45 a
PPM Group	40.90 ± 1.05	45.43 ± 1.79
GBP-PRF Group	44.83 ± 1.09	48.43 ± 0.45 a
PPM-PRF Group	41.67 ± 0.68	43.37 ± 0.52 b

Adhesion Score	GBP Group			PPM Group			GBP-PRF Group			PPM-PRF Group		
	W 4	W 8	W 12	W 4	W 8	W 12	W 4	W 8	W 12	W 4	W 8	W 12
0	--	--	--	--	--	--	--	--	2	--	--	1
1	1	2	3	--	--	1	3	2	1	1	2	2
2	1	1	--	--	2	1	--	1	--	2	1	--
3	1	--	--	2	1	1	--	--	--	--	--	--
4	--	--	--	1	--	--	--	--	--	--	--	--

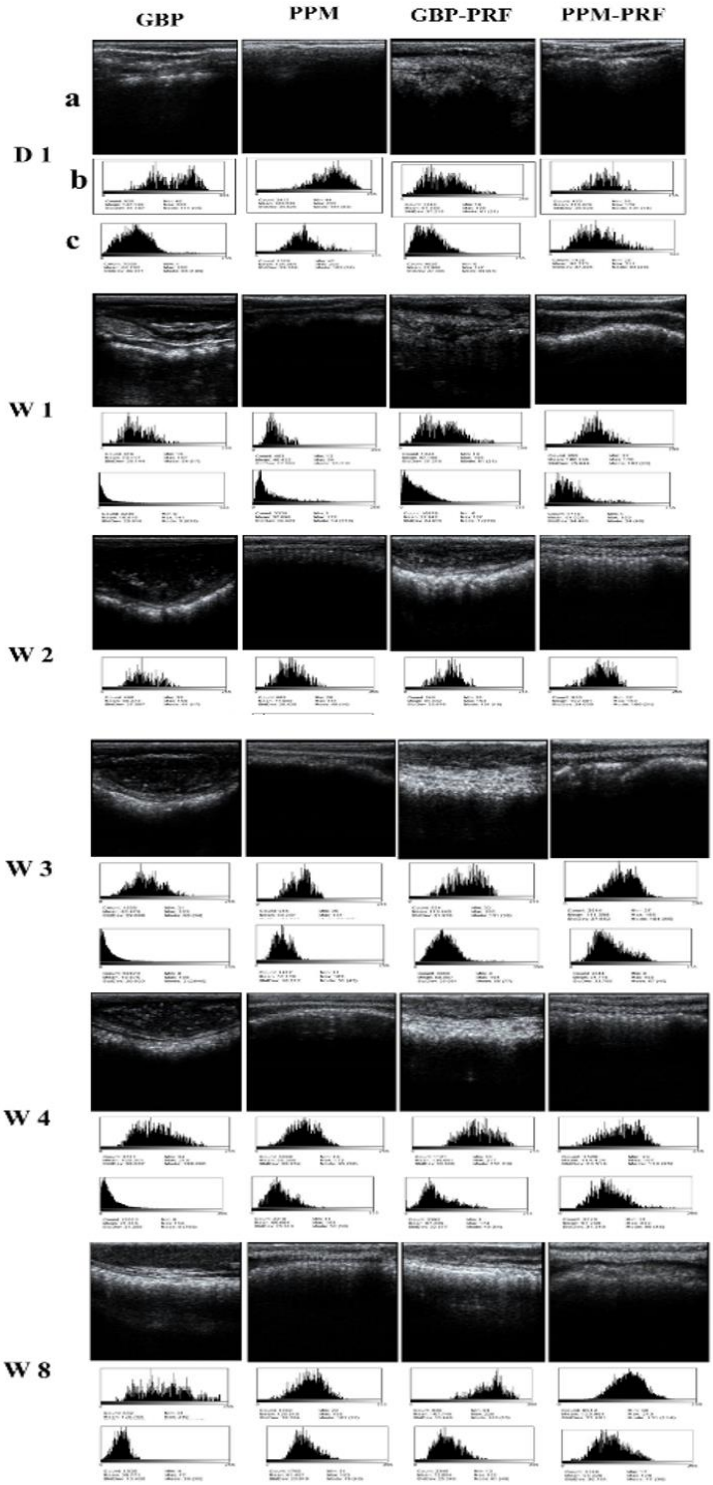
GBP
PPM
GBP-PRF
PPM-PRF
a
D 1
b
c
W 1
W 2
W 3
W 4
W 8

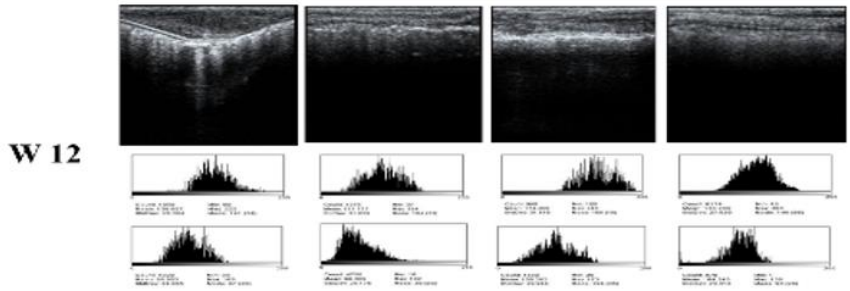
W 12

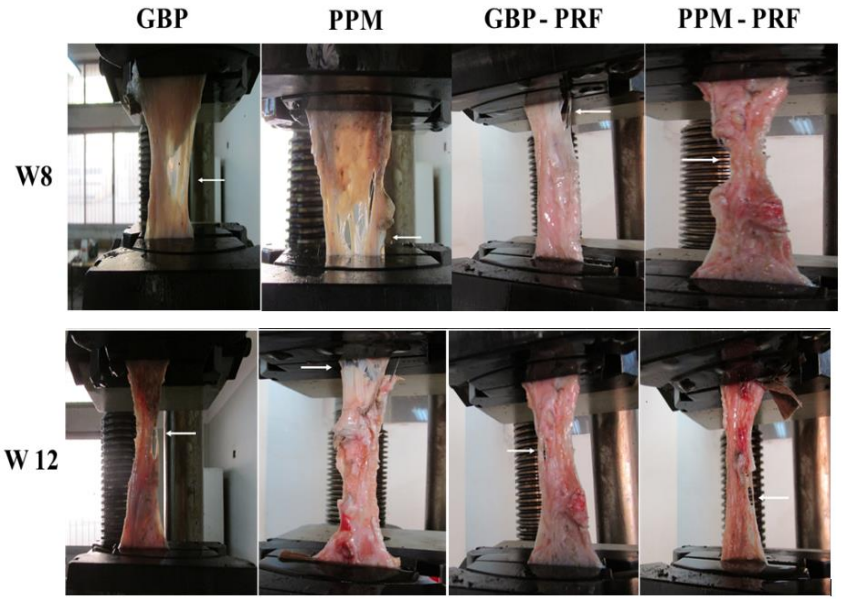
GBP
PPM
GBP - PRF
PPM - PRF
W8
W 12

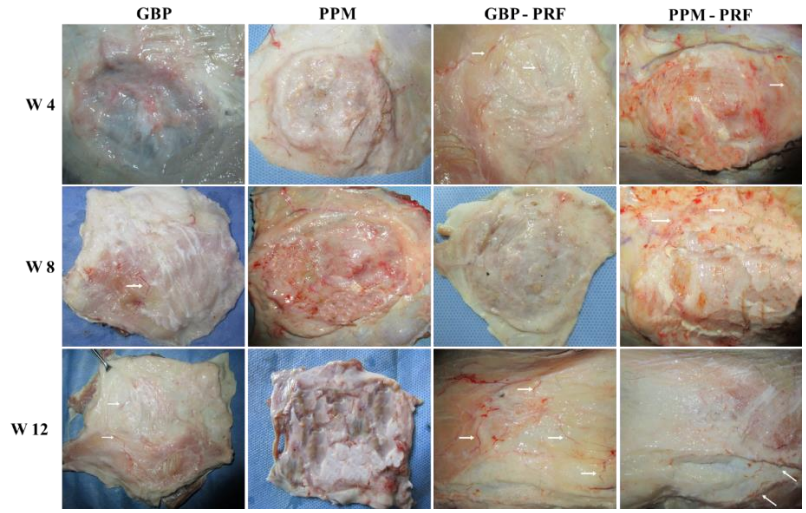
GBP
PPM
GBP - PRF
PPM - PRF
W 4
W 8
W 12

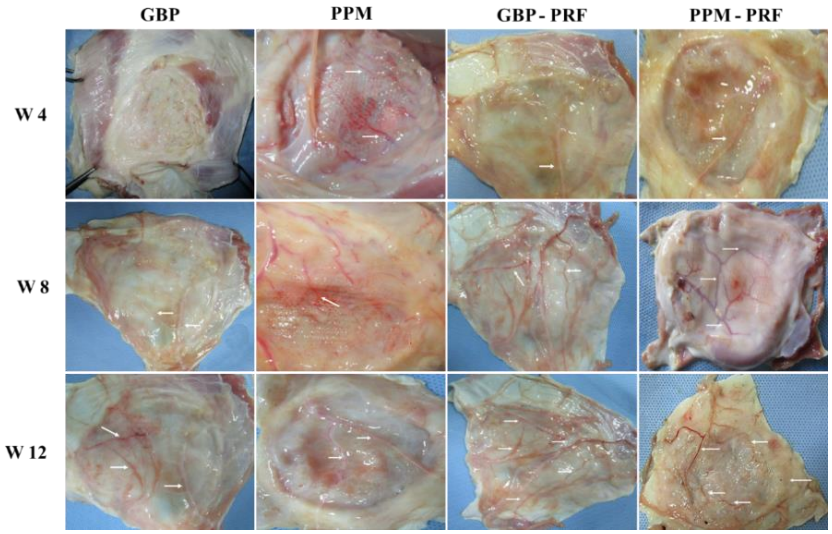
GBP
PPM
GBP - PRF
PPM - PRF
W 4
W 8
W 12

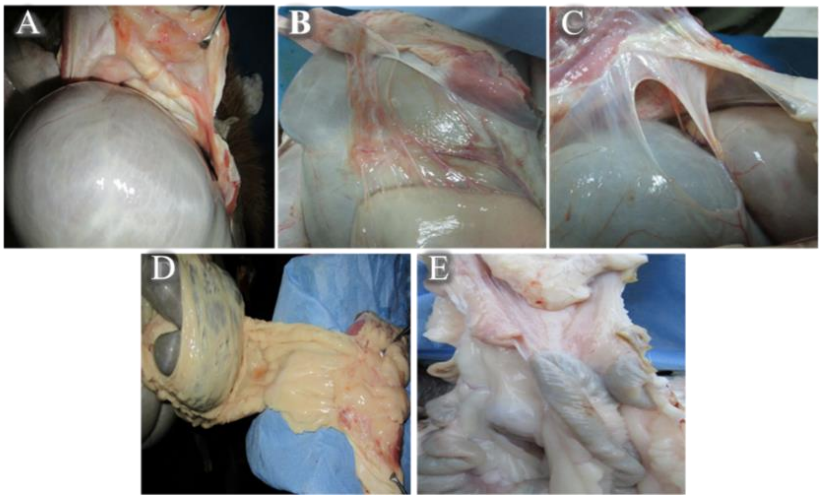
A
B
C
D
E

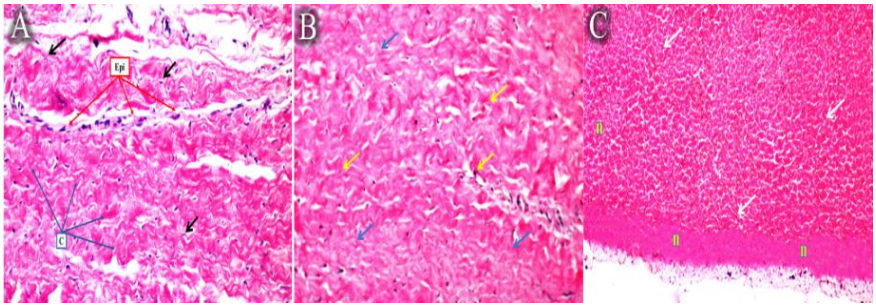
A
B
C

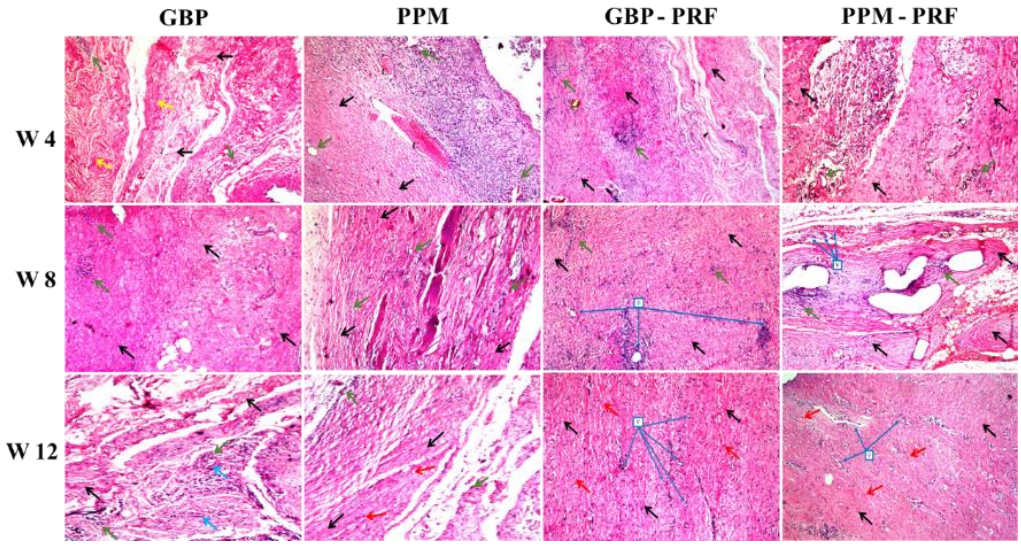
GBP
PPM
GBP - PRF
PPM - PRF
W 4
W 8
W 12

Predictive Potential for 7 CpG Differentially Methylated in Saliva Samples Markers According to GEO-Projects

Viachaslau Kipen

Dr., Institute of Genetics and Cytology of the National Academy of Sciences of Belarus, Minsk/Belarus

Maryna Bahdanava

Dr., Institute of Genetics and Cytology of the National Academy of Sciences of Belarus, Minsk/Belarus

Valiantsina Lemesh

Assoc. Prof. Dr., Institute of Genetics and Cytology of the National Academy of Sciences of Belarus, Minsk/Belarus

Abstract

Based on the data presented in publicly available on GEO-NCBI platform 8 by definition genome-wide DNA methylation projects using Infinium Human Methylation 450K BeadChip (Illumina ©) - GSE59505, GSE72120, GSE72556, GSE78874, GSE92767, GSE99029, GSE110128, GSE111223, - with the total number of residents 690 (without the presence of chronic and acute diseases in history) we calculated the correlation coefficients for 7 CpG-markers cg18384097 (*PTPN7* gene), cg00481951 (*SST* gene), cg19671120 (*CNGA3* gene), cg14361627 (*KLF14* gene), cg08928145 (*TSSK6* gene), cg12757011 (*TBR1* gene), cg07547549 (*SLC12A5* gene) and the coefficients of determination and comparison characteristics multivariate linear regression equations. We have shown that for residents without a history of chronic or acute illness, regardless of ethno-geographical and gender factors, CpG markers cg00481951 (*SST* gene) and cg14361627 (*KLF14* gene) have the greatest predictive potential for determining chronological age, with cumulative analysis 10 GEO projects account for 62.9-74.5% and 62.7-73.8% of the variance of the variable "Age, Number of Years", respectively. When analyzing all 7 CpG markers, the variability of the variable "Age, Number of Years" explained within the regression model varies between 75.9-94.5% (when analyzing GEO projects in the context of the ethnographic origin of residents).

Keywords: chronological age, DNA methylation, epigenetic markers, saliva, buccal epithelium

Introduction

Determining chronological age from biological fluid samples and tissue fragments plays an important role in forensic practice: it can limit the search for identification of remains, help narrow the range of suspects, thereby saving time, which is often the limiting factor for a successful investigation. Due to the importance of the problem of ensuring the safety of citizens of the Union State (Russian Federation and the Republic of Belarus), the development of age determination technologies for changing lifetime DNA modifications is undoubtedly relevant.

To solve the problem of determining the chronological age of a person, the most reliable, namely reproducible, linearly dependent, sensitive and specific, and economically justified is the approach to determining the chorological age based on identifying the level of DNA methylation at specific CpG sites (Goel, Karir, & Garg, 2017; Hannum et al., 2013).

One of the most common biological forensic samples is the buccal epithelium (or saliva). The world has proposed several methods for determining the age of an individual: according to the level of intravital chemical modification (methylation) of selected sections of his DNA, differing in the number of genetic loci under investigation and the method of analysis, with a claimed accuracy of up to 3-12 years, depending on the number of sections used in the analysis and technologies (Alghanim et al., 2017; Alsaleh, McCallum, Halligan, & Haddrill, 2017; Bocklandt et al., 2011; Horvath, 2013; Horvath et al., 2014, 2015; Horvath & Ritz, 2015; Koch & Wagner, 2011; Lee, Lee, & Shin, 2016; Park et al., 2016; Rana, 2018; Sparrow et al., 2016; (1) Zbieć-Piekarska et al., 2015). However, the applicability of these methods for determining the age of representatives of the population of the regions of the Union State has not been established, because, as shown in a

number of studies, the methylation level of specific CpGs may vary depending on the ethnogeographical origin of the residents under study (Fleckhaus et al., 2017).

In order to improve the accuracy of methods for determining the age of an individual by the level of methylation of selected DNA segments, it is necessary to verify the techniques based on known DNA segments, including representatives of various ethnogeographical groups of the population of the Union State and to identify specific population groups, the inclusion of which in the techniques will allow determining the chronological age with an acceptable level of error for problems of forensic science.

Modern methods for studying DNA methylation at the genome level imply the use of one of two technological platforms for high-throughput analysis of nucleotide sequences - DNA hybridization on microchips (microarray), or parallel clonal DNA sequencing (Massive parallel sequencing - MPS or Next generation sequencing - NGS). Hybridization microchips remain the most popular platform for genomic analysis of DNA methylation. Comparatively low costs compared to full-genome sequencing positioned microchips as a tool convenient for studying differentially methylated regions based on analysis of the methylation status of known CpG sites of the human genome.

At the beginning of 2019, Illumina © is releasing for research the third generation of hybridization chips for analyzing the full genome profile of human DNA methylation, Infinium Methylation EPIC BeadChip, followed by the first (Infinium Human Methylation 27 BeadChip, IHM 27K BeadChip) and the second (Infinium Human Methylation 450K BeadChip, IHM 450K BeadChip) generations.

However, it is for IHM 450K BeadChip that the largest amount of primary data (in the form of methylation level expressed in % or unit fraction) is accumulated as for various types of biological samples (blood, separate cell fractions of blood, buccal epithelium (saliva), semen), and for different ethnic groups or patients with a history of chronic diseases (cancer, diabetes, metabolic syndrome, arterial hypertension). The IHM 450K BeadChip platform is designed to analyze the methylation state of 482421 CpG sites and covers 99% of the RefSeq genes (an average of 17 CpG dinucleotides per gene).

Biological age is representative of the degree of morphological and physiological development of the organism, in the context of DNA methylation has a trend different from linear. This fact is due to a number of reasons (Freire-Aradas et al., 2016; Horvath, 2013; Smeers et al., 2018; (2) Zbieć-Piekarska et al., 2015): hyper- and / or hypofunctional gene expression in the process of intensive growth of the organism during the pre-pubertal and early puberty periods, the presence of chronic diseases (bronchial asthma, multiple sclerosis, epilepsy, diabetes mellitus, cancer and others), normal gerontological processes, the presence of bad habits (smoking, excessive alcohol consumption), etc. Deviations in the change of methylation profile from the linear trend for biological age, associated with the growth and the aging of the body, most pronounced in the age of 18-23 years and after 60 years. The discrepancies between chronological and biological age, which make it possible to assess the intensity of aging and the functionality of the individual, are ambiguous in different phases of the aging process. However, the accuracy of a linear trend (multiple linear regression is enough to predict age with a high accuracy in a wide age range.

The goal of research work within the framework of the Union State Scientific and Technical Program “Development of innovative geno-geographical and genomic technologies for identifying individuals and individual human characteristics based on studying gene pools of Union State regions” (“DNA Identification”), Activity No 2 “Development of a method for determining the probable age of an individual characteristic of its DNA” (Minsk, Republic of Belarus) at the first stage is the analysis of the current state of science in research and the development of possible approaches to determining the age of an unknown individual based on the intravital chemical modification (methylation) of selected sections of its DNA.

Thus, the purpose of this work is to calculate the values of the correlation coefficients (R) and determination (R^2) for 7 CpG markers cg18384097 (*PTPN7* gene), cg00481951 (*SST* gene), cg19671120 (*CNGA3* gene), cg14361627 (*KLF14* gene), cg08928145 (*TSSK6* gene), cg12757011 (*TBR1* gene), cg07547549 (*SLC12A5* gene) in the context of various ethnogeographical groups.

Materials and methods

DNA samples. The total number of buccal epithelium samples included in the study, for which the methylation level was determined using IHM 450K BeadChip, was 872 samples. Information on the methylation level (expressed in % or fractions of a unit) for samples of buccal epithelium was made publicly available on NCBI GEO datasets platform (Gene Expression Omnibus, https://www.ncbi.nlm.nih.gov/gds) for the following projects : GSE59505 (Lee et al., 2015) (2014; executing

country - South Korea) - 6 samples (practically healthy residents); GSE72120 (Sparrow et al., 2016) (2015, Great Britain) - 72 samples (newborns with no signs of pathology in the anamnesis); GSE72556 (2015, USA) - 96 samples (children of preschool age with no pathology in the anamnesis); GSE78874 (Horvath & Gurven, 2016) (2016, USA) - 259 samples (practically healthy residents); GSE92767 (Hong et al., 2017) (2016, South Korea) - 54 samples (practically healthy residents); GSE99029 (Gopalan et al., 2017) (2017, USA) - 57 samples (practically healthy residents); GSE110128 (Langie et al., 2018) (2018, Belgium) - 53 samples (33 patients with allergic disorders and 20 practically healthy residents); GSE111223 (Chuang et al., 2017; Horvath & Ritz, 2015) (2018, USA) - 259 samples (128 patients with Parkinson's disease and 131 practically healthy residents).

The number of practically healthy residents of various ethnographic origin was 690 people, with a history of acute or chronic diseases - 182 people. The range of chronological age according to 10 GEO projects for residents included in the study ranged from 1 month (for newborns) to 91 years. The number of samples of buccal epithelium from men was 391, from women - 299.

Selection of CpG markers for modeling. In the analysis, it was decided to use the information on those 7 CpG markers that proposed as a test system for determining the chronological age of Sae Rom Hong et al. (Hong et al., 2017): cg18384097 (*PTPN7* gene, protein tyrosine phosphatase, non-receptor type 7, NCBI Gene ID - 5778), cg00481951 (*SST* gene, somatostatin, NCBI Gene ID - 280932), cg19671120 (*CNGA3* gene, cyclic nucleotide gated channel alpha 3, NCBI Gene ID - 1261), cg14361627 (*KLF14* gene, Kruppel like factor 14, NCBI Gene ID - 136259), cg08928145 (*TSSK6* gene, testis specific serine kinase 6, NCBI Gene ID - 83983), cg12757011 (*TBR1* gene, T -box, brain 1, NCBI Gene ID - 10716), cg07547549 (*SLC12A5* gene, solute carrier family 12 member 5, NCBI Gene ID - 57468).

Statistical data analysis. The Spearman rank correlation coefficient was calculated using the bootstrap function on the number of 1000 runs, and calculated the 95% confidence interval in software SPSS v.20.0.

The coefficient of determination (R^2), as well as the corrected R^2, equal to the fraction of the variance of the dependent chronological age variable due to the influence of independent variables representing the methylation level of 7 CpG markers, were calculated using software SPSS v.20.0.

Results and discussion

As a rule, projects for assessing a genome-wide methylation profile using the IHM 450K BeadChip are aimed at a cohort of people who represent a specific cross-section of the population of a particular regional or ethnicity. Thus, in the overwhelming majority of scientific works, researchers are focused on finding dependencies between the DNA methylation profile and whether a disease is applied to tasks within a particular state or geographical region. This fact makes it possible to carry out within the framework of this work comparative study and characterize the correlation coefficients for the seven CpG-markers - cg18384097 (*PTPN7* gene), cg00481951 (*SST* gene), cg19671120 (*CNGA3* gene), cg14361627 (*KLF14* gene), cg08928145 (*TSSK6* gene) cg12757011 (*TBR1* gene), cg07547549 (*SLC12A5* gene), depending on a number of factors, namely: the gender of the residents (male or female); ethnoregional affiliation within the European (UK, Belgium), North American (US) and East Asian (South Korea) regions.

Correlation coefficients in the framework of independent GEO-projects. The correlation coefficients (R) for 7 CpG markers calculated in 4 NCBI GEO projects (provided that the number of conditionally healthy residents was at least 50 people) - GSE78874 (n = 259), GSE92767 (n = 54), GSE99029 (n = 57), GSE111223 (n = 131), are presented in table 1 (Appendixe). In the analysis, information was used only for practically healthy residents, without specifying the ethogeographic or gender factor.

For the CpG marker cg18384097 (*PTPN7* gene), the R values were in the range [(-0.278) - 0.163] with an average value (calculated according to 8 projects) R_{mean} = [0.031]; for cg00481951 (*SST* gene) - [0.323 - 0.905], R_{mean} = [0.762]; cg19671120 (*CNGA3* gene) - [0.308 - 0.813], R_{mean} = [0.736]; cg14361627 (*KLF14* gene) - [0.362 - 0.875], R_{mean} = [0.754]; cg08928145 (*TSSK6* gene) - [0.116 - 0.729], R_{mean} = [0.674]; cg12757011 (*TBR1* gene) - [0.292 - 0.796], R_{mean} = [0.669]; cg07547549 (*SLC12A5* gene) - [0.375 - 0.812], R_{mean} = [0.759].

The largest difference for the calculated R-values was shown for CpG markers: for cg08928145 (*TSSK6* gene) ABS (module) = 0.613; for cg00481951 (*SST* gene), 0.582; for cg14361627 (*KLF14* gene) - 0.513. The minimum difference for the calculated R-values was shown for the CpG marker cg07547549 (*SLC12A5* gene), ABS = 0.437. Thus, the most reproducible R-values in 4 independent GEO projects were shown for CpG markers cg07547549 (*SLC12A5* gene) and cg12757011 (*TBR1* gene).

Correlation coefficients depending on the ethnogeographical origin. Correlation coefficients (R) for 7 CpG markers calculated in the framework of 6 NCBI GEO projects are presented in Table 2 (Appendixe). The analysis used information only for practically healthy residents, taking into account ethnogeographical origin and without specifying a gender factor. The number of persons belonging to the "Korean-Asian" group was 60 (GSE59505, South Korea, n = 6; GSE92767, South Korea n = 54), to the group "Bantu / European" - 57 (GSE99029, United Kingdom), to the group "Hispanic / Mexican" - 236 (GSE72556, USA, n = 96; GSE78874, USA, n = 93; GSE111223, USA, n = 47), to the group "Caucasian / European" - 376 (GSE72120, United Kingdom, n = 72; GSE39560, Germany, n = 34; GSE110128, Belgium, n = 20; GSE111223, USA, n = 84; GSE78874, USA, n = 166).

For the CpG marker cg18384097 (*PTPN7* gene), the R-values were in the range [(-0.335) - 0.163]; for cg00481951 (*SST* gene) - [0.446 - 0.907]; cg19671120 (*CNGA3* gene) - [0.428 - 0.799]; cg14361627 (*KLF14* gene) - [0.510 - 0.842]; cg08928145 (*TSSK6* gene) - [0.266 - 0.790]; cg12757011 (*TBR1* gene) - [0.448 - 0.711]; cg07547549 (*SLC12A5* gene) - [0.539 - 0.813].

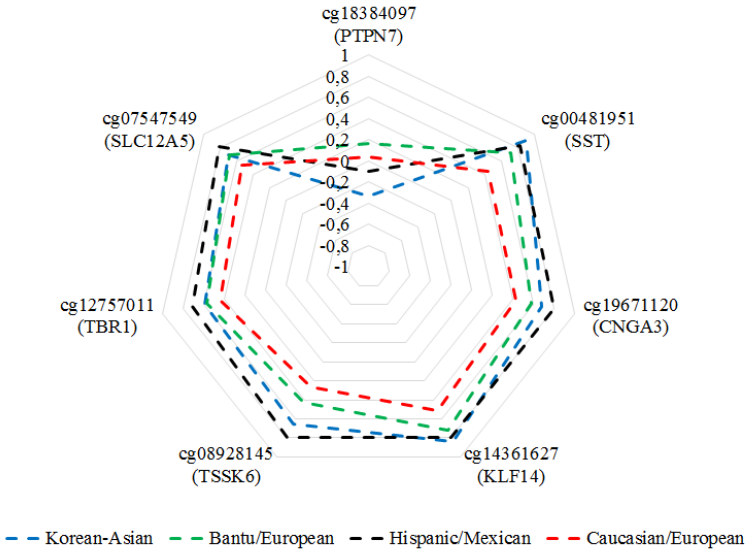

Fig. 1. Correlation coefficients for 7 CpG markers, calculated depending on the ethnoregional origin of residents according to 6 GEO projects ("Korean-Asian", n = 60; "Bantu / European", n = 57; "Hispanic / Mexican", n = 236; "Caucasian / European", n = 376)

The largest difference for the calculated R-values was shown for CpG markers: for cg08928145 (*TSSK6* gene) ABS (module) = 0.524; for cg00481951 (*SST* gene) - 0.461; for cg19671120 (*CNGA3* gene) - 0.371. The minimum difference for the calculated R-values was shown for the CpG marker cg12757011 (*TBR1* gene), ABS = 0.263. Thus, the most reproducible R-values in 9 independent GEO projects were shown for CpG markers cg07547549 (*SLC12A5* gene) and cg12757011 (*TBR1* gene).

T***he correlation coefficients depending on the gender factor***. The correlation coefficients (R) for 7 CpG markers, calculated in the framework of 6 NCBI GEO projects (provided that the number of conditionally healthy residents of each gender was at least 50 people): for the "Caucasian / European" group - GSE110128, GSE111223, GSE39560, GSE72120, GSE78874 (M = 180, F = 196); for the groups "Hispanic / Mexican" and "Latino" - GSE111223, GSE72556, GSE78874 (M = 129, F = 104) - are presented in table 3 (Appendixe), fig. 2 and 3. In the analysis, information was used only for practically healthy residents taking into account gender and ethnogeographical concretization. The total number of males (sample "M") was 309 people, female (sample "F") - 300 people.

For the CpG marker cg18384097 (*PTPN7* gene), the R-values for sample “M” were in the range [(-0.335) - 0.071] with an average value (calculated according to 7 projects - GSE90167, GSE71223, GSE7505) R^{M}_{mean} = [0.066; p = 0,230]; for cg00481951 (*SST* gene) - [0.382 - 0.907] with R^{M}_{mean} = [0.778; p = 7.22E-68]; for cg19671120 (*CNGA3* gene) - [0.434 -

0.677)] with R^{M}_{mean} = [0.766; p = 1.19E-64]; for cg14361627 (*KLF14* gene) - [0.453 - 0.842] with R^{M}_{mean} = [0.781; p = 1.14E-68]; for cg08928145 (*TSSK6* gene) - [0.339 - 0.773] with R^{M}_{mean} = [0.720; p = 1,11E-53]; for cg12757011 (*TBR1* gene) - [0.502] with R^{M}_{mean} = [0.695; p = 1.16E-48]; for cg07547549 (*SLC12A5* gene) - [0.596 - 0.809] with R^{M}_{mean} = [0.812; p = 2.84E-78], Fig.2.

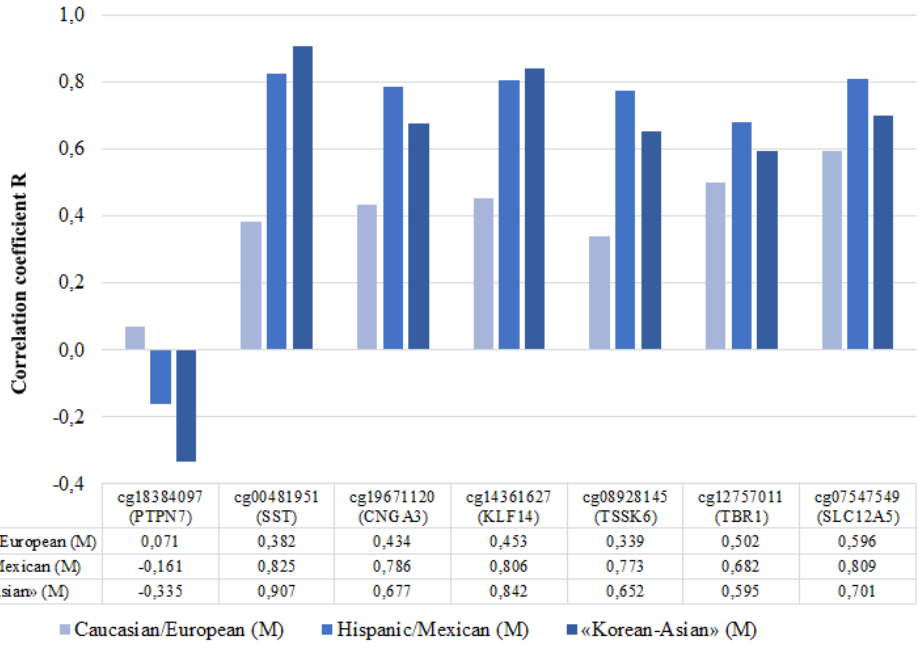

	cg18384097 (PTPN7)	cg00481951 (SST)	cg19671120 (CNGA3)	cg14361627 (KLF14)	cg08928145 (TSSK6)	cg12757011 (TBR1)	cg07547549 (SLC12A5)
Caucasian/European (M)	0,071	0,382	0,434	0,453	0,339	0,502	0,596
Hispanic/Mexican (M)	-0,161	0,825	0,786	0,806	0,773	0,682	0,809
«Korean-Asian» (M)	-0,335	0,907	0,677	0,842	0,652	0,595	0,701

Fig. 2. Correlation coefficients for 7 CpG markers calculated depending on the ethnoregional origin of male residents according to 6 GEO projects ("Korean-Asian", n = 60; "Hispanic / Mexican", n = 129; "Caucasian / European", N = 180)

For CpG marker cg18384097 (*PTPN7* gene), R values for sample “F” were in the range [(-0.236) - 0.008] with an average value (calculated according to 6 projects - GSE110128, GSE111223, GSE39560, GSE72120, GSE72556, GSE78874) R^{F}_{mean} = [-0.046; p = 0.497]; for cg00481951 (*SST* gene) - [0.557 - 0.774] with R^{F}_{mean} = [0.838; p = 2.27E-71]; for cg19671120 (*CNGA3* gene) - [0.379 - 0.726] with R^{F}_{mean} = [0.792; p = 1.44E-58]; for cg14361627 (*KLF14* gene) - [0.562 - 0.691] with R^{F}_{mean} = [0.817; p = 3.54E-65]; for cg08928145 (*TSSK6* gene) - [0.200 - 0.740] with R^{F}_{mean} = [0.735; 2.08E-46]; for cg12757011 (*TBR1* gene) - [0.387 - 0.632] with R^{F}_{mean} = [0.759; p = 4.71E-51]; for cg07547549 (*SLC12A5* gene) - [0.426 - 0.740] with R^{F}_{mean} = [0.793; p = 1,22E-58], Fig.3.

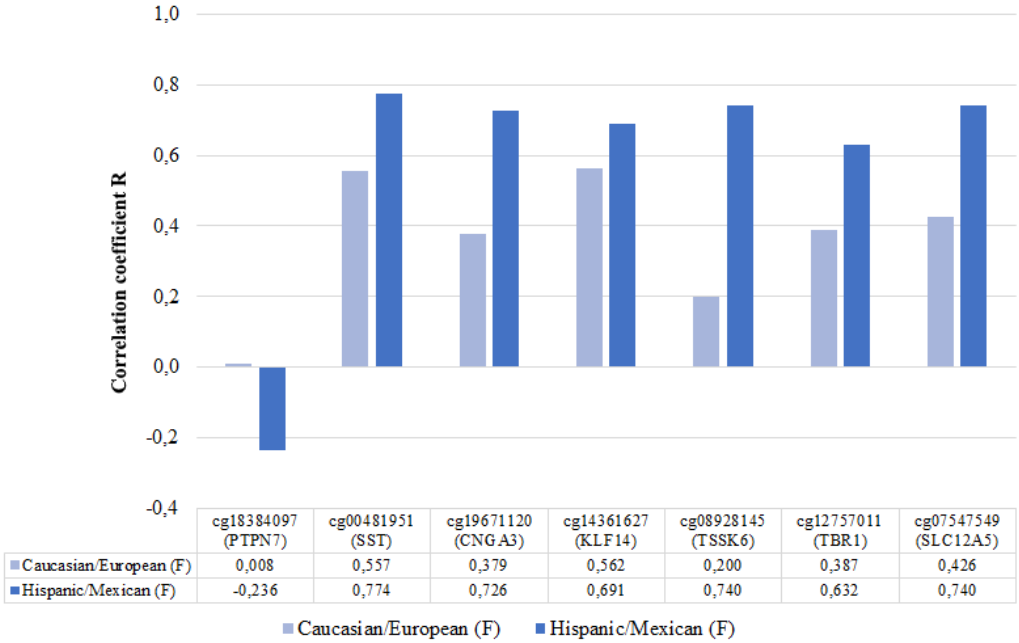

	cg18384097 (PTPN7)	cg00481951 (SST)	cg19671120 (CNGA3)	cg14361627 (KLF14)	cg08928145 (TSSK6)	cg12757011 (TBR1)	cg07547549 (SLC12A5)
Caucasian/European (F)	0,008	0,557	0,379	0,562	0,200	0,387	0,426
Hispanic/Mexican (F)	-0,236	0,774	0,726	0,691	0,740	0,632	0,740

Fig. 3. Correlation coefficients for 7 CpG markers calculated depending on the ethnoregional origin of female residents according to 6 GEO-projects ("Hispanic / Mexican", n = 104; "Caucasian / European", n = 196)

The largest difference for the calculated R-values for the "M" sample was shown for CpG markers: cg00481951 (*SST* gene) ABS (module) = 0.525; cg08928145 (*TSSK6* gene) - 0.434; cg14361627 (*KLF14* gene) - 0.389. The largest difference for the calculated R-values for the sample "F" was shown for CpG markers: cg08928145 (*TSSK6* gene) ABS (module) = 0.540; cg19671120 (*CNGA3* gene) - 0.347; cg07547549 (*SLC12A5* gene) - 0.314. The minimum difference for the calculated R values for both samples ("M" and "F") was shown for the CpG marker cg19671120 (*CNGA3* gene), ABS = 0.005, cg12757011 (*TBR1* gene) - 0.065 and cg07547549 (*SLC12A5* gene) - 0.101.

Calculation of coefficients of determination (R ^ 2) for 7 CpG markers. We calculated the adjusted determination coefficients for multiple linear regression both for individual GEO projects (according to table 1 (Appendixe)) and in the context of ethnogeographical status (according to table 2 (Appendixe)) based on the data on the methylation level of 7 CpG markers. Based on the data presented in Fig. 4, it is clear that if the mean age values in the sample were shifted to a more age (> 60 years) range (for example, for projects GSE78874 or GSE111223), then the corrected R^2 was less. It is known that regression model is capable of adequately (with a calculated level of accuracy) predicting a dependent variable (chronological age) when modeling only in the analyzed range of values, therefore, the extension of the age range for the dependent variable is able to stabilize the model.

When combining several GEO projects into groups depending on the resident's belonging to a particular ethnic group, it was shown that the coefficients of determination (R ^ 2) varied in the range of 0.759-0.945, Figure 5.

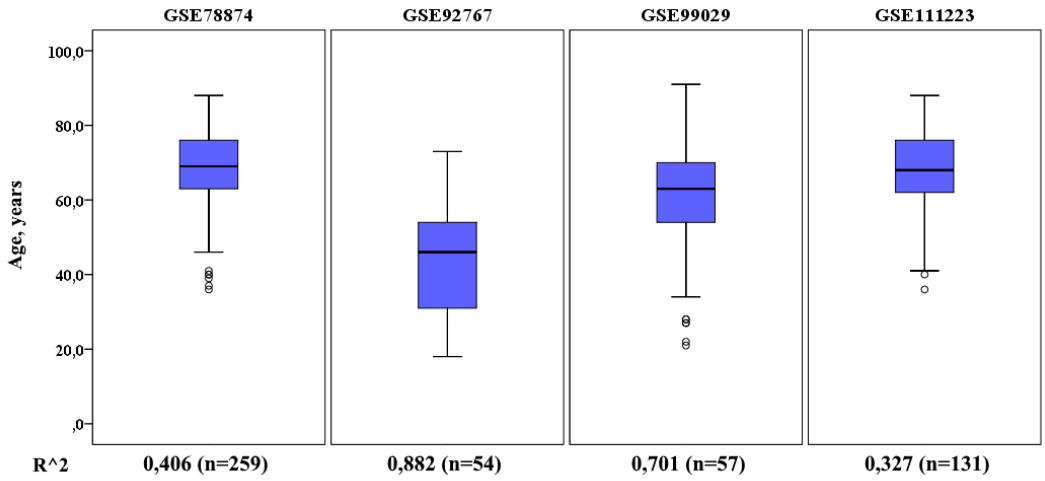

Fig. 4. Characteristics of the analyzed GEO-projects by age included in the study of residents (for projects from Table 1). Below are the values of the corrected coefficients of determination R^2 for chronological age, calculated according to 7 CpG markers

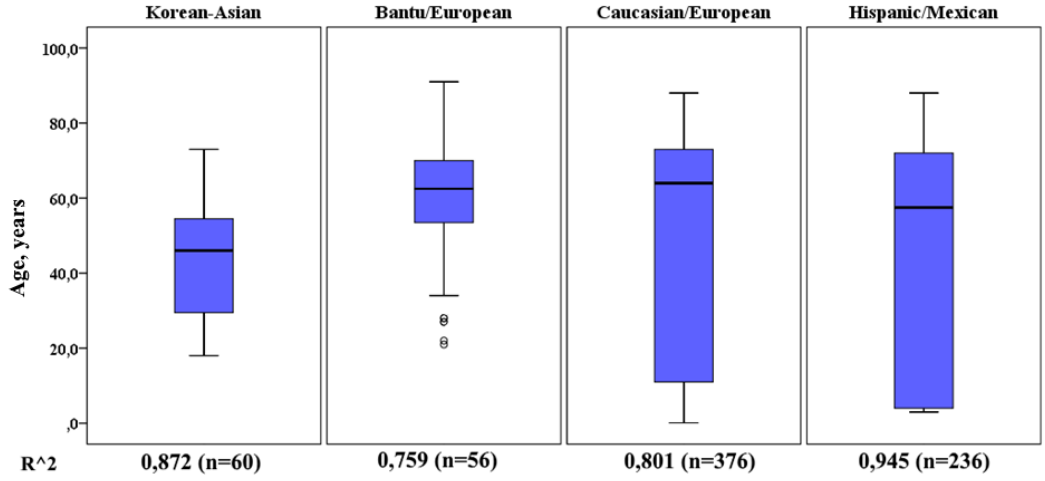

Fig. 5. Characteristics of the analyzed GEO-projects by age included in the study of residents (for projects from Table 2). Below are the values of the corrected coefficients of determination R^2 for chronological age, calculated according to 7 CpG markers

For each group of residents, in the context of ethnicity, the equations of multiple linear regression were calculated - Fig.6. Figure 6-A shows the true and adjusted predicted values of chronological age for each ethnic group, calculated on the basis of the methylation level of 7 CpG markers. In fig. 6-B - the same data, only when adjusted for the gender of residents. Thus, when the gender variable factor is included in the regression equation, the accuracy of prediction of chronological age increases, but only slightly. Depending on the ethnicity of residents, the inclusion of the variable “Gender” in the analysis can increase the accuracy of the model by 0.4–4.6%.

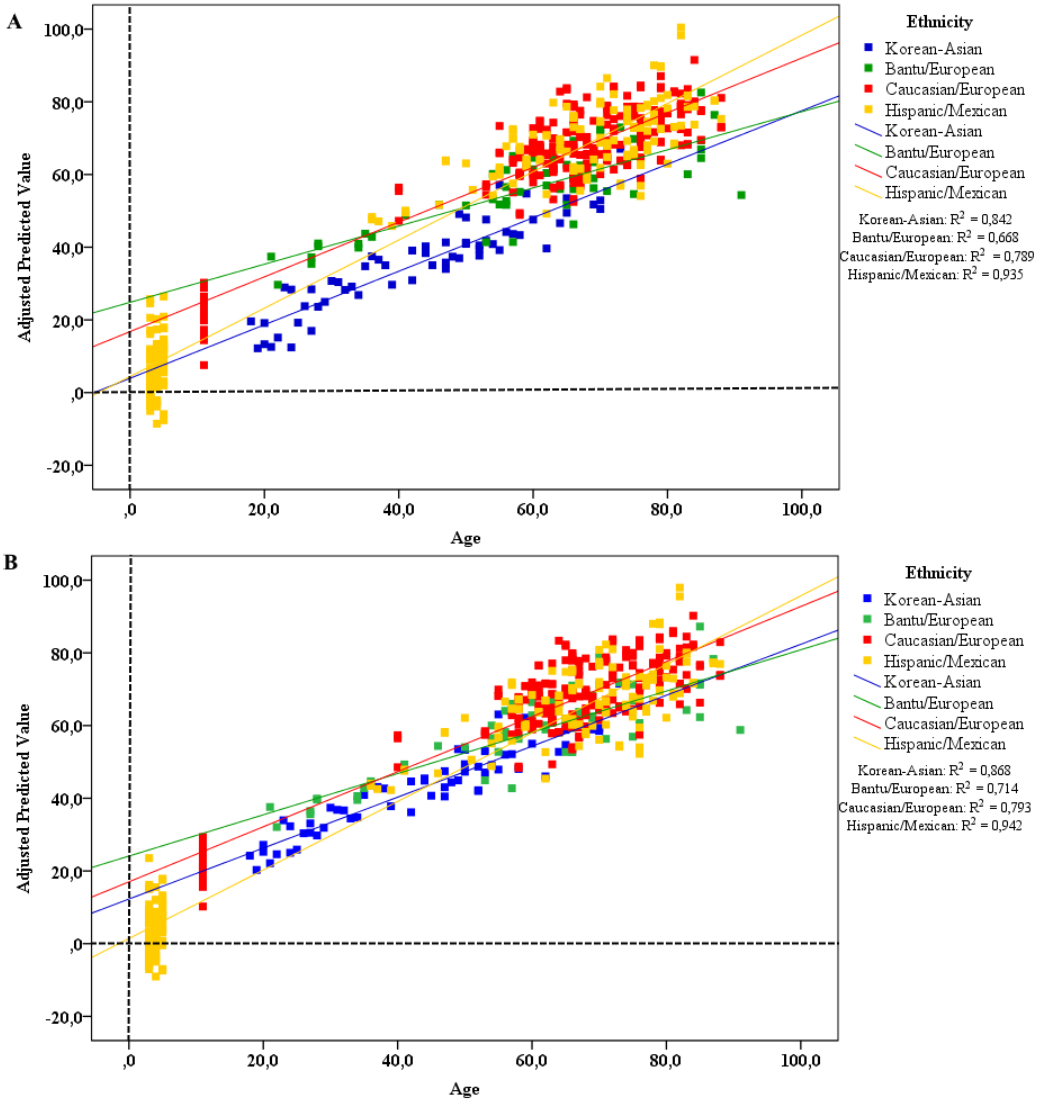

Fig. 6. Regression model for prediction of chronological age by the level of methylation of CpG markers: A - according to 7 CpG markers; B - according to 7 CpG markers (taking into account the gender factor)

As part of the cumulative analysis of the data of 8 GEO-projects on the impact on the change of the coefficient of determination (R^2), the CpG markers are arranged in the following sequence: cg00481951 (R^2 = 0.776), cg14361627 (+0.047 to the previous value of R^2) cg18384097 (+0.035), cg19671120 (+0.029), cg07547549 (+0.005), cg12757011 (+0.001), cg08928145 (+0.001). For residents of the “Caucasian / European” group, the CpG markers are arranged in the following sequence (only significant changes of R^2 are shown): cg07547549 (R^2 = 0.579), cg00481951 (+0.131), cg18384097 (+0.039), cg14361627 (+0.043), cg19671120 (+0.011), cg12757011 (+0.004); for residents of the “Hispanic/Mexican” group: cg00481951 (R^2 = 0.887), cg14361627 (+0.037), cg19671120 (+0.007), cg18384097 (+0.012), cg07547549 (+0.003); for the Bantu / European group: cg14361627 (R^2 = 0.727), cg00481951 (+0.036), cg19671120 (+0.020).

In general, in addition to information on the level of methylation of CpG markers, the availability of additional data (gender, ethnicity, the presence of chronic diseases, the presence of bad habits) that can be included in the regression model equation, we believe, can improve the accuracy of prediction of chronological age. Attracting results from GEO projects and expanding the database on which the model is built can also increase the accuracy of the analysis.

Conclusion

Based on the data presented in publicly available on GEO-NCBI platform 8 by definition genome-wide DNA methylation projects using Infinium Human Methylation 450K BeadChip (Illumina ©) - GSE59505, GSE72120, GSE72556, GSE78874, GSE92767, GSE99029, GSE110128, GSE111223, - with the total number of residents 690 (without the presence of chronic and acute diseases in history) we calculated the correlation coefficients for 7 CpG-markers cg18384097 (*PTPN7* gene), cg00481951 (*SST* gene), cg19671120 (*CNGA3* gene), cg14361627 (*KLF14* gene), cg08928145 (*TSSK6* gene), cg12757011 (*TBR1* gene), cg07547549 (*SLC12A5* gene) and the coefficients of determination and comparison characteristics multivariate linear regression equations.

We have shown that for residents without a history of chronic or acute illness, regardless of ethno-geographical and gender factors, CpG markers cg00481951 (*SST* gene) and cg14361627 (*KLF14* gene) have the greatest predictive potential for determining chronological age, with cumulative analysis all GEO projects account for 62.9-74.5% and 62.7-73.8% of the variance of the variable “Age, Number of Years”, respectively. When analyzing all 7 CpG markers, the variability of the variable “Age, Number of Years” explained within the regression model varies between 75.9-94.5% (when analyzing GEO projects in the context of the ethnographic origin of residents).

Thus, the scheme for determining the chronological age by identification the methylation profile by 7 CpG markers is characterized by universality, i.e. regardless of the ethnogeographical status of an unknown person or his gender, it is possible to give criminologists sufficiently accurate (limited to the accuracy of the model used for the analysis) information on the individual's estimated age or on what age group he belongs to.

In general, to increase the accuracy of predicting chronological age using the CpG marker methylation profile for an unidentified person from a specific geographic region, or taking into account the ethnic, national or gender component, as well as taking into account information on the presence of chronic or acute diseases, the use of additional specific CpG markers.

Age determination technology based on DNA methylation profiles is developed within the framework of the Scientific and Technical Program of the Union State Scientific and Technical Program “Development of innovative geno-geographical and genomic technologies for identifying individuals and individual human characteristics based on studying gene pools of Union State regions” (“DNA Identification”) in the context of Activity No. 2 “Development of a method for determining the probable age of an individual characteristic of its DNA”. It will be based on the results of advanced global and fundamental, exploratory scientific research, scientific and technical, industrial, technological, organizational and legal developments and will ensure the use of new knowledge in the field of applied genetics in solving forensic tasks in the territory of the Republic of Belarus and the Russian Federation.

References

[1] Alghanim, H., Antunes, J., Silva, D. S. B. S., Alho, C. S., Balamurugan, K., & McCord, B. (2017). Detection and evaluation of DNA methylation markers found at SCGN and KLF14 loci to estimate human age. Forensic Science International. Genetics, 31, 81–88. https://doi.org/10.1016/j.fsigen.2017.07.011

[2] Alsaleh, H., McCallum, N. A., Halligan, D. L., & Haddrill, P. R. (2017). A multi-tissue age prediction model based on DNA methylation analysis. Forensic Science International: Genetics Supplement Series, 6, e62–e64. https://doi.org/10.1016/j.fsigss.2017.09.056

[3] Bocklandt, S., Lin, W., Sehl, M. E., Sánchez, F. J., Sinsheimer, J. S., Horvath, S., & Vilain, E. (2011). Epigenetic predictor of age. PloS One, 6(6), e14821. https://doi.org/10.1371/journal.pone.0014821

[4] Chuang, Y.-H., Paul, K. C., Bronstein, J. M., Bordelon, Y., Horvath, S., & Ritz, B. (2017). Parkinson’s disease is associated with DNA methylation levels in human blood and saliva. Genome Medicine, 9(1), 76. https://doi.org/10.1186/s13073-017-0466-5

[5] Fleckhaus, J., Freire-Aradas, A., Rothschild, M. A., & Schneider, P. M. (2017). Impact of genetic ancestry on chronological age prediction using DNA methylation analysis. Forensic Science International: Genetics Supplement Series, 6, e399–e400. https://doi.org/10.1016/j.fsigss.2017.09.162

[6] Freire-Aradas, A., Phillips, C., Mosquera-Miguel, A., Girón-Santamaría, L., Gómez-Tato, A., Casares de Cal, M., … Lareu, M. V. (2016). Development of a methylation marker set for forensic age estimation using analysis of public methylation data and the Agena Bioscience EpiTYPER system. Forensic Science International. Genetics, 24, 65–74. https://doi.org/10.1016/j.fsigen.2016.06.005

[7] Goel, N., Karir, P., & Garg, V. K. (2017). Role of DNA methylation in human age prediction. Mechanisms of Ageing and Development, 166, 33–41. https://doi.org/10.1016/j.mad.2017.08.012

[8] Gopalan, S., Carja, O., Fagny, M., Patin, E., Myrick, J. W., McEwen, L. M., … Henn, B. M. (2017). Trends in DNA Methylation with Age Replicate Across Diverse Human Populations. Genetics, 206(3), 1659–1674. https://doi.org/10.1534/genetics.116.195594

[9] Hannum, G., Guinney, J., Zhao, L., Zhang, L., Hughes, G., Sadda, S., … Zhang, K. (2013). Genome-wide methylation profiles reveal quantitative views of human aging rates. Molecular Cell, 49(2), 359–367. https://doi.org/10.1016/j.molcel.2012.10.016

[10] Hong, S. R., Jung, S.-E., Lee, E. H., Shin, K.-J., Yang, W. I., & Lee, H. Y. (2017). DNA methylation-based age prediction from saliva: High age predictability by combination of 7 CpG markers. Forensic Science International. Genetics, 29, 118–125. https://doi.org/10.1016/j.fsigen.2017.04.006

[11] Horvath S., Gurven M., Levine M.E. et al. (2016) An epigenetic clock analysis of race/ethnicity, sex, and coronary heart disease. Genome Biol. 2016. 11. e1-e22. https://doi.org/10.1186/s13059-016-1030-0

[12] Horvath, S. (2013). DNA methylation age of human tissues and cell types. Genome Biology, 14(10), R115. https://doi.org/10.1186/gb-2013-14-10-r115

[13] Horvath, S., & Ritz, B. R. (2015). Increased epigenetic age and granulocyte counts in the blood of Parkinson's disease patients. Aging, 7(12), 1130–1142. https://doi.org/10.18632/aging.100859

[14] Horvath, S., Erhart, W., Brosch, M., Ammerpohl, O., von Schönfels, W., Ahrens, M., … Hampe, J. (2014). Obesity accelerates epigenetic aging of human liver. Proceedings of the National Academy of Sciences of the United States of America, 111(43), 15538–15543. https://doi.org/10.1073/pnas.1412759111

[15] Horvath, S., Garagnani, P., Bacalini, M. G., Pirazzini, C., Salvioli, S., Gentilini, D., … Franceschi, C. (2015). Accelerated epigenetic aging in Down syndrome. Aging Cell, 14(3), 491–495. https://doi.org/10.1111/acel.12325

[16] Koch, C. M., & Wagner, W. (2011). Epigenetic-aging-signature to determine age in different tissues. Aging, 3(10), 1018–1027. https://doi.org/10.18632/aging.100395

[17] Langie, S. A. S., Moisse, M., Szarc Vel Szic, K., Van Der Plas, E., Koppen, G., De Prins, S., … De Boever, P. (2018). GLI2 promoter hypermethylation in saliva of children with a respiratory allergy. Clinical Epigenetics, 10, 50. https://doi.org/10.1186/s13148-018-0484-1

[18] Lee H. Y., An J. H., Jung S. E., et al. (2015) Genome-wide methylation profiling and a multiplex construction for the identification of body fluids using epigenetic markers. Forensic Sci. Int. Genet. 17. 17-24. DOI: 10.1016/j.fsigen.2015.03.002

[19] Lee, H. Y., Lee, S. D., & Shin, K.-J. (2016). Forensic DNA methylation profiling from evidence material for investigative leads. BMB Reports, 49(7), 359–369.

[20] Park, J.-L., Kim, J. H., Seo, E., Bae, D. H., Kim, S.-Y., Lee, H.-C., … Kim, Y. S. (2016). Identification and evaluation of age-correlated DNA methylation markers for forensic use. Forensic Science International. Genetics, 23, 64–70. https://doi.org/10.1016/j.fsigen.2016.03.005

[21] Rana, A. K. (2018). Crime investigation through DNA methylation analysis: methods and applications in forensics. Egyptian Journal of Forensic Sciences, 8(1), 7. https://doi.org/10.1186/s41935-018-0042-1

[22] Smeers, I., Decorte, R., Van de Voorde, W., & Bekaert, B. (2018). Evaluation of three statistical prediction models for forensic age prediction based on DNA methylation. Forensic Science International. Genetics, 34, 128–133. https://doi.org/10.1016/j.fsigen.2018.02.008

[23] Sparrow, S., Manning, J. R., Cartier, J., Anblagan, D., Bastin, M. E., Piyasena, C., … Boardman, J. P. (2016). Epigenomic profiling of preterm infants reveals DNA methylation differences at sites associated with neural function. Translational Psychiatry, 6, e716. https://doi.org/10.1038/tp.2015.210

[24] Zbieć-Piekarska, R., Spólnicka, M., Kupiec, T., Makowska, Ż., Spas, A., Parys-Proszek, A., … Branicki, W. (2015). Examination of DNA methylation status of the ELOVL2 marker may be useful for human age prediction in forensic science. Forensic Science International. Genetics, 14, 161–167. https://doi.org/10.1016/j.fsigen.2014.10.002

[25] Zbieć-Piekarska, R., Spólnicka, M., Kupiec, T., Parys-Proszek, A., Makowska, Ż., Pałeczka, A., … Branicki, W. (2015). Development of a forensically useful age prediction method based on DNA methylation analysis. Forensic Science International. Genetics, 17, 173–179. https://doi.org/10.1016/j.fsigen.2015.05.001

Appendixes

Table 1. Correlation coefficients (R) for 7 CpG, calculated in the framework of 8 projects of NCBI GEO (separately included calculations for those projects for which the number of conditionally healthy residents is at least 50 people)

Project NCBI GEO (number of samples)	R (95% CI), p-level	CpG-markers						
		cg18384097 (*PTPN7*)	cg00481951 (*SST*)	cg19671120 (*CNGA3*)	cg14361627 (*KLF14*)	cg08928145 (*TSSK6*)	cg12757011 (*TBR1*)	cg07547549 (*SLC12A5*)
8 projects # (n=842)	LL 95%	-0,051	0,710	0,685	0,707	0,619	0,616	0,709
	R	**0,031**	**0,762**	**0,736**	**0,754**	**0,674**	**0,669**	**0,759**
	HL 95%	0,112	0,807	0,783	0,798	0,720	0,712	0,800
	p-level	0,4418	1,4E-115	6,3E-104	7,6E-112	5,67E-81	1,86E-79	6,4E-114
GSE78874 (n=259)	LL 95%	-0,102	0,296	0,181	0,243	0,053	0,159	0,248
	R	0,024	**0,419**	**0,308**	**0,362**	**0,177**	**0,292**	**0,375**
	HL 95%	0,154	0,536	0,428	0,473	0,295	0,418	0,498
	p-level	0,7001	3,74E-12	6,05E-07	3,19E-09	0,004922	2,37E-06	7,71E-10
GSE92767 (n=54)	LL 95%	-0,534	0,805	0,685	0,764	0,525	0,667	0,678
	R	**-0,278**	**0,905**	**0,813**	**0,875**	**0,729**	**0,796**	**0,812**
	HL 95%	0,014	0,956	0,890	0,933	0,862	0,877	0,906
	p-level	0,0419	5,72E-21	7,72E-14	5,11E-18	4,23E-10	6,05E-13	8,79E-14
GSE99029 (n=57)	LL 95%	-0,132	0,515	0,311	0,478	0,151	0,309	0,451
	R	0,163	**0,721**	**0,573**	**0,717**	**0,431**	**0,575**	**0,693**
	HL 95%	0,429	0,872	0,756	0,875	0,670	0,756	0,858
	p-level	0,2263	2,44E-10	3,26E-06	3,49E-10	0,000814	2,89E-06	2,29E-09
GSE111223 (n=131)	LL 95%	-0,086	0,155	0,158	0,250	-0,055	0,118	0,215
	R	0,102	**0,323**	**0,324**	**0,408**	0,116	**0,304**	**0,384**
	HL 95%	0,279	0,494	0,486	0,557	0,296	0,471	0,537
	p-level	0,2658	0,0003	0,0003	3,39E-06	0,2052	0,0007	1,35E-05

Note: # - GSE110128, GSE111223, GSE59505, GSE72120, GSE72556, GSE78874, GSE92767, GSE99029; LL 95% - the lower limit of the 95% confidence interval; HL 95% - upper limit of 95% confidence interval; ND - no data

Table 2. Correlation coefficients (R) for 7 CpG, calculated in the framework of 9 NCBI GEO projects, for which the number of conditionally healthy residents belonging to a particular ethnic group was at least 50 people

Project NCBI GEO (number of samples)	R (95% ДИ), p-level	CpG-markers						
		cg18384097 (*PTPN7*)	cg00481951 (*SST*)	cg19671120 (*CNGA3*)	cg14361627 (*KLF14*)	cg08928145 (*TSSK6*)	cg12757011 (*TBR1*)	cg07547549 (*SLC12A5*)
«Caucasian/European»[1] (n=376)	LL 95%	-0,091	0,320	0,297	0,399	0,124	0,318	0,422
	R	0,039	**0,446**	**0,428**	**0,510**	**0,266**	**0,448**	**0,539**
	HL 95%	0,162	0,556	0,536	0,600	0,388	0,553	0,630
	p-level	0,5313	4,94E-14	6,63E-13	1,78E-18	1,46E-05	3,66E-14	8,07E-21
«Hispanic/Mexican»[2] (n=236)	LL 95%	-0,235	0,787	0,751	0,741	0,740	0,639	0,765
	R	-0,101	**0,830**	**0,799**	**0,792**	**0,790**	**0,711**	**0,813**
	HL 95%	0,029	0,864	0,834	0,834	0,827	0,768	0,851
	p-level	0,1289	2,47E-59	7,44E-52	2,68E-50	7,36E-50	2,17E-36	4,66E-55
«Korean-Asian»[3] (n=60)	LL 95%	-0,564	0,827	0,452	0,721	0,397	0,329	0,493
	R	**-0,335**	**0,907**	**0,677**	**0,842**	**0,652**	**0,595**	**0,701**
	HL 95%	-0,084	0,949	0,834	0,912	0,812	0,803	0,844
	p-level	0,0088	1,77E-23	2,77E-09	3,23E-17	1,72E-08	5,3E-07	4,43E-10
«Bantu/European» (n=57)	LL 95%	-0,131	0,501	0,306	0,458	0,146	0,323	0,455
	R	0,163	**0,721**	**0,573**	**0,717**	**0,431**	**0,575**	**0,693**
	HL 95%	0,436	0,870	0,763	0,880	0,652	0,758	0,856
	p-level	0,2263	2,44E-10	3,26E-06	3,49E-10	0,000814	2,89E-06	2,29E-09

Note: 1 - GSE110128, GSE111223, GSE72120, GSE78874, GSE39560; 2– GSE111223, GSE72556, GSE78874; 3 - GSE59505, GSE92767; 4 - GSE99029; LL 95% - the lower limit of the 95% confidence interval; HL 95% - upper limit of 95% confidence interval

Table 3. Correlation coefficients (R) for 7 CpG, calculated in the framework of 6 projects of NCBI GEO depending on the gender of the residents (calculations for those projects for which the number of conditionally healthy residents was at least 50)

Ethnic group NCBI GEO (кол-во образцов)	R (95% ДИ), p-level	CpG-markers						
		cg18384097 (*PTPN7*)	cg00481951 (*SST*)	cg19671120 (*CNGA3*)	cg14361627 (*KLF14*)	cg08928145 (*TSSK6*)	cg12757011 (*TBR1*)	cg07547549 (*SLC12A5*)
«Caucasian/European»[1] (M*=180)	LL 95%	-0,104	0,218	0,275	0,288	0,192	0,346	0,461
	R	0,071	**0,382**	**0,434**	**0,453**	**0,339**	**0,502**	**0,596**
	HL 95%	0,229	0,539	0,573	0,589	0,479	0,630	0,699
	p-level	0,4024	2,98E-06	7,46E-08	1,66E-08	4E-05	2,36E-10	6,36E-15
«Caucasian/European»[2] (F**=196)	LL 95%	-0,189	0,399	0,189	0,410	-0,021	0,175	0,236
	R	0,008	**0,557**	**0,379**	**0,562**	**0,200**	**0,387**	**0,426**
	HL 95%	0,219	0,697	0,557	0,689	0,387	0,567	0,591
	p-level	0,9293	6,69E-11	2,55E-05	4,24E-11	0,0305	1,62E-05	1,63E-06
«Hispanic/Mexican»[3] (M=129)	LL 95%	-0,344	0,758	0,704	0,737	0,683	0,562	0,726
	R	-0,161	**0,825**	**0,786**	**0,806**	**0,773**	**0,682**	**0,809**
	HL 95%	0,024	0,874	0,840	0,856	0,828	0,784	0,862
	p-level	0,0697	7,69E-33	6,71E-28	3,36E-30	2,02E-26	1,02E-18	1,22E-30
«Hispanic/Mexican»[3] (F=104)	LL 95%	-0,236	**0,774**	**0,726**	**0,691**	**0,740**	**0,632**	**0,740**
	R	-0,015	0,844	0,795	0,779	0,803	0,724	0,816
	HL 95%	0,188	0,894	0,842	0,844	0,850	0,792	0,863
	p-level	0,879443	1,62E-28	3E-23	9,15E-22	5,55E-24	1,27E-17	2,74E-25
«Korean-Asian»[4] (M=60)	LL 95%	-0,564	0,827	0,452	0,721	0,397	0,329	0,493
	R	**-0,335**	**0,907**	**0,677**	**0,842**	**0,652**	**0,595**	**0,701**
	HL 95%	-0,084	0,949	0,834	0,912	0,812	0,803	0,844
	p-level	0,0088	1,77E-23	2,77E-09	3,23E-17	1,72E-08	5,3E-07	4,43E-10

Note: 1 - GSE110128, GSE111223, GSE72120, GSE78874; 2 - GSE110128, GSE111223, GSE39560, GSE72120, GSE78874; 3– GSE111223, GSE72556, GSE78874; 4 - GSE59505, GSE92767; * - men; ** - women; LL 95% - the lower limit of the 95% confidence interval; HL 95% - upper limit of 95% confidence interval

The Effect of DNAase Activity of Pseudomonas Aeruginosa, Causative Agents of Pyelonephritis, on the Ability to Form Biofilms

Malanchuk Svitlana
Department of general and clinical immunology and allergology of V. N. Karazin Kharkiv National University, Kharkiv, Ukraine

Mishina Marina
Department of microbiology, virology and immunology name by D.P. Grinev of Kharkov National Medical University, Kharkiv, Ukraine

Hololobova Olesia
Department of general and clinical immunology and allergology of V. N. Karazin Kharkiv National University, Kharkiv, Ukraine

Abstract

Pseudomonas aeruginosa is one of the leading causative agents of purulent-inflammatory infections with a high mortality rate, including pyelonephritis, what mainly depends on the ability to produce pathogenic enzymes and form a dense biofilms. Therefore, the study of the influence of the DNase activity of Pseudomonas aeruginosa on the ability to form biofilms will allow the development of new approaches to the diagnosis of infections, taking into account the biological properties of the pathogen. As a result of the study, it was found that 85,7% of Pseudomonas aeruginosa strains isolated in acute form of pyelonephritis had a high degree of DNase activity and the remaining 14,3% of Pseudomonas aeruginosa isolates had a moderate degree of DNase activity. The strains of Pseudomonas aeruginosa, isolated from patients with chronic pyelonephritis in 85,3% of cases were weakly DNase active, and the remaining isolates did not have DNase activity at all. After determining the ability of clinical strains of Pseudomonas aeruginosa to form daily biofilms, it was shown that isolates of acute form of pyelonephritis form biofilms of density 2,08 ± 0,26 u.opt. dens., whereas isolates of chronic pyelonephritis form biofilms of density 4,59 ± 0,23 u. opt. dens. and actively produced planktonic cells. It was established that the clinical strains of Pseudomonas aeruginosa, isolated from the acute form of pyelonephritis, form lower density biofilms, however, have higher DNase activity compared to chronic pyelonephritis isolates, which form more dense biofilms, although their planktonic cells have weak DNase activity.

Keywords: Pseudomonas aeruginosa, biofilms, DNase activity.

Neutrophiles Phagocytic Activity and NETs Forming Ability in Young Children with Acute Pyelonephritis

Maryna Mishyna
Prof., MD, Chief of D.P. Grynyov Department of Microbiology, Virology and Immunology, Kharkiv National Medical University, Kharkiv

Iryna Marchenko
PhD student of D.P. Grynyov Department of Microbiology, Virology and Immunology, Kharkiv National Medical University, Kharkiv, Ukraine

Yuliya Mozgova
Assoc. Prof.of D.P. Grynyov Department of Microbiology, Virology and Immunology, Kharkiv National Medical University, Kharkiv, Ukraine

Abstract

The study of the neutrophils functional reserves as the basis for protective and adaptive capabilities of the organism allows us to predict the development of immunodeficiency in acute pyelonephritis in young children that is necessary for timely adjustments to treatment. The study was provided to determine the number of active neutrophils, the phagocytic number and the neutrophil count before the formation of NETs in young children with acute pyelonephritis. It was established that mentioned indexes varied depending on the causative agent of acute pyelonephritis. The highest quantity of activated neutrophils (92.9 ± 0.77 %), phagocytic number (8.4 ± 0.15 conditional units) and antigen quantity in NETs (27.5 ± 0.7 conditional units) took place in *E. faecalis* etiology. The indexes for E. coli were slightly lower and appropriately folded 82.2 ± 1.4 %, 5.9 ± 0.19 and 18.0 ± 0.5 conditional units. In the case of *K. pneumoniae* quantity of activated neutrophils was 70.4 ± 4.7 %, phagocytic number – 4.5 ± 1.2 and antigen quantity in NETs – 15.0 ± 1.2 conditional units that indicates a change in phagocytic activity of the immune defense in children with acute pyelonephritis. The decrease in the phagocytosis and the quantity of absorbed *K. pneumoniae* antigens in NETs is due to the formation of a capsule. It is shown that quantity of activated neutrophils, activity of phagocytosis and ability to catch antigens in NETs in young children with acute pyelonephritis depends on etiology and pathogenicity factors of causative agent and needs further research.

Keywords: neutrophils, phagocytic index, NETs, microorganisms, young children, acute pyelonephritis.